NUMERICAL INVESTIGATION OF STEADY STATE AND TRANSIENT THERMAL PERFORMANCE OF A MULTI-CHIP VAPOR CHAMBER

by

MOHAMMAD PARHIZI

Presented to the Faculty of the Graduate School of

The University of Texas at Arlington in Partial Fulfillment

of the Requirements

for the Degree of

MASTER OF SCIENCE IN MECHANICAL ENGINEERING

THE UNIVERSITY OF TEXAS AT ARLINGTON

May 2015

Acknowledgements

First and foremost, I would like to express my sincere appreciation and gratitude to my advisor Dr. Jain. I would like to thank him for his excellent guidance, help and support. I have been extremely lucky to have the opportunity to work with Dr. Jain who cared so much about my work, and provided insights to break through the problems.

Also, I would like to acknowledge with much appreciation the crucial role of Dr. Merrikh on this dissertation and thank him for his brilliant comments, encouraging words, thoughtful criticism and suggestions.

Also, I would like to thank all my professors, especially Dr. Moon and Dr. Agonafer for serving in my defense committee and for their support and encouragement.

I will forever be thankful to my parents, for their unconditional love, for actually believing in me and for sending inspiration and support across the world. I would not be where I am today if it wasn't for them.

Last but not least, my very special thanks to my sister and brother in law for their constant love, inspiration and support over the past 2 years.

April 16, 2015

Abstract

NUMERICAL INVESTIGATION OF STEADY STATE AND TRANSIENT THERMAL PERFORMANCE OF A MULTI-CHIP VAPOR CHAMBER

Mohammad Parhizi, M.S

The University of Texas at Arlington, 2015

Supervising Professor: Ankur Jain

Effective dissipation of heat generated in microelectronic devices during operation is critical for reliability and performance, particularly for advanced architectures such as microserver chips. Vapor chambers are a class of heat spreaders that have received much recent attention due to their passive nature and superior heat spreading capability. Several studies have investigated thermal performance of vapor chambers as heat spreading devices. However, developing a simple and accurate model which could be easily used in industry is still a big challenge. Moreover, more work needs to be done to optimize the performance of vapor chambers. For instance, developing a vapor chamber model for the increasingly common scenario of multiple chips and investigating the effects of heat density and chip orientation on the vapor chamber performance may provide designers with an opportunity to optimize the performance of these heat spreading devices.

In this thesis, first, a simplified pure conduction model is developed to investigate thermal performance of a vapor chamber integrated with a single high power chip. Vapor chamber components are modeled as solid layers with effective thermal conductivities. Then, the single high power chip is replaced with a system of multiple lower power chips.

The performance of the vapor chamber integrated with multiple lower power chips is compared with the single chip scenario. Results imply that due to a considerable reduction in junction temperature in multiple chips scenario, reducing the vapor space or copper wall thickness may result in a cost saving design opportunity of a vapor chamber with same functionality as the single chip scenario.

Next, a multi-physics steady state and transient numerical simulation of a vapor chamber is carried out for both single and multiple chips scenarios. The model is capable of accounting for fluid motion in the wick structure. The performance of this model is compared with the simplified pure conduction model from the previous section. By inclusion of the fluid flow phenomena, the model is expected to predict the vapor chamber performance more realistically. Also, a study is conducted to investigate the effects of heat density and chip orientation on the performance of the vapor chamber.

This work is expected to facilitate the quantification of thermal performance of vapor chambers and feasibility evaluation for future semiconductor thermal management needs. The model presented here captures salient physics, yet is simple enough to be used for thermal management design for semiconductor devices.

The sensitivity study conducted in this work provides important information about the effect of different design parameters variables on vapor chamber performance. These contributions are expected to facilitate the adoption of vapor chamber technology in thermal management of semiconductor device.

Table of Contents

List of Illustrations

List of Tables

Chapter 1

Introduction

Due to the need for enhanced functionality and higher performance in electronics industry, microserver chips are experiencing increasingly larger heat fluxes. Local heat density on some chips may approach 100-200 W/cm^2. The resulting high temperatures lead to poor performance, decreased reliability and decreased lifetime.

To meet the desirable reliability and performance, it is critical to ensure that the junction temperature is kept in a range between 85 to100˚C. Per every 2˚C increment in the normal operating temperature, the reliability of electronic components drops by 10% [1]. Therefore, advanced heat spreaders with high heat transfer characteristics are needed for heat dissipation from electronic components.

The use of vapor chambers and heat pipes instead of traditional solid heat spreaders has often been considered. The motivation behind this is that the phase change which occurs inside vapor chambers provides higher effective thermal conductivity as compared to solids. Passive nature, low thermal resistance, low space requirement, simple structure and effective heat transport are among the advantages of flat vapor chambers. Owing to these advantages, vapor chambers and flat heat pipes received significant attention for various applications. Initially, the need for an effective way to transfer heat in space applications led to the development of heat pipes. Since heat conduction is limited in vacuum, heat pipes were developed to transport large amount of heat in low gravity and low temperature difference conditions by the means of convective heat transfer. Today, the application of vapor chambers and heat pipes are extended to thermal management of electronic devices [2,3], renewable energy [4] applications and air conditioning systems [5]. Reviews of the heat pipes and vapor chambers applications can be found in [6,7].

A vapor chamber consists of a porous domain and vapor space surrounded by a metal enclosure. The porous domain, called the wick, consists of a thin layer of sintered copper saturated in working fluid. Depends on the application, required operating temperature and the wall material, different types of liquids such as water, methanol, acetone, ammonia, sodium and lithium can be used as working fluid in vapor chambers. Although vapor chambers come in different sizes and thickness, the total thickness of a thin vapor chamber is usually less than 5 mm. The lower copper boundary is attached to a heat source and the upper copper boundary is attached to the heat sink where air- or liquid cooling techniques may be applied. Figure 1-1 shows the schematic of the structure of a typical vapor chamber.

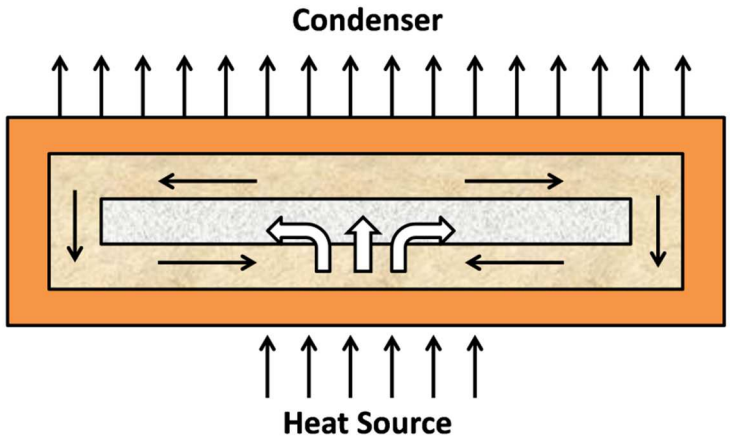

Figure 1-1: Schematic of the Structure of a Vapor Chamber

During the operation, the lower wall absorbs heat from the microprocessor chip and transfers it to the wick structure by conduction. The working fluid inside the wick structure absorbs the heat and evaporates. The vapor carries the heat and moves toward the vapor space due to the pressure difference. Heat is then transferred from the vapor to the upper wall resulting in vapor condensation. The upper wall eventually rejects the heat to the ambient. The condensed liquid returns to the wick structure by capillary action and

results in a passive cooling operation. To maintain this cyclical operation, capillary pressure in the wick structure must overcome the cumulative viscous and inertial pressure drop along the vapor and liquid flow paths. Figure 1-2 schematically shows fluid motion inside the vapor chamber.

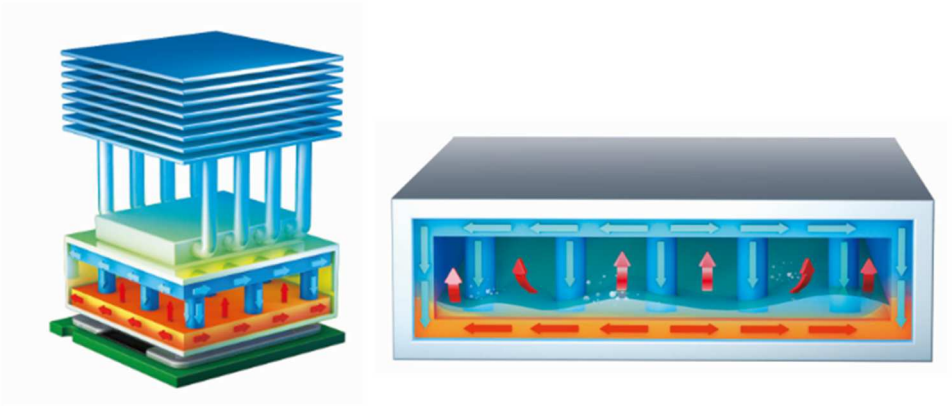

Figure 1-2: Fluid Flow inside Vapor Chamber [8]

Among the mechanisms mentioned above, phase change between liquid and vapor has much stronger effect on heat transfer process than heat conduction of the solid components. It implies that the overall thermal resistance of the vapor chamber is mainly contributed by the solid components.

Operation of a vapor chamber involves several fluid flow and heat transfer mechanisms such as phase change heat transfer, flow through the porous media, capillary flow and multiphase fluid flow which create a highly coupled problem. Therefore, thermal management of a vapor chamber is a very complicated problem to solve not only analytically but also using numerical methods. There are several simulation software available for numerical purposes. However, some of the assumptions and boundary conditions for this problem are not available in current software. For example, phase

change from liquid to vapor occurs at the wick-vapor core interface which is not a usual interface condition in available software.

This thesis investigates the thermal management of a vapor chamber integrated with single and multiple heat sources. Chapter 2 reviews the literature and discusses the researches that have been done on vapor chambers and heat pipes in the past. In Chapter 3, a simplified conduction model is developed for the vapor chamber and the results are presented for both single and multiple chips scenario. In chapter 4, a multi-physics vapor chamber model which captures the fluid flow in wick structure is presented. Steady state and transient thermal performance of the vapor chamber is investigated. Performance of this model is compared with the pure conduction model from chapter 3, copper and aluminum heat spreaders. The effects of heat density and chip orientation on the vapor chamber performance are studied. Results and limitations of the model are highlighted.

Chapter 2

Background and Literature Review

2.1 Background Theory of Heat Pipes

Some of the important terms of the theory of heat pipes which are used to develop the pure conduction model introduced in chapter 3 and operation limits will be discussed briefly in this section.

2.1.1 Theory of Heat Pipes

Some of the general terms of the theory of heat pipes are presented in this section. Comprehensive explanations of the theory of heat pipes can be found in [2,9].

The maximum heat carrying capacity of a heat pipe or in other word, the capillary limit is determined by the pressure drop in the liquid and vapor phase. The capillary driving force must be greater than the vapor and liquid pressure drop for the heat pipe to operate [2].

Low temperature drop in the vapor results in a high thermal conductivity in heat pipes. Temperature drop in the vapor can be estimated from the pressure drop model and the Clausius-Clapeyron equation [2,11].

The thermal resistance of the wick structure is high. Also, there is no need to solve the fluid flow inside the wick structure to calculate the thermal resistance of the heat pipe components [2,11].

2.1.2 Limitations

There are several factors which may limit the operation of a heat pipe. In other word, several phenomena may occur during the operation of a heat pipe and results in constraint on the maximum heat carrying capacity of the heat pipe. Comprehensive explanation of the limitations on the performance of heat pipes can be found in [2,9]. Some of these limitations are briefly explained in this section.

1) Capillary Limit

Depends on the working fluid, wick structure and permeability, the ability of a capillary structure to circulate the liquid has a certain limit. This limit is also called the hydrodynamic limitation. It occurs when the maximum capillary pressure of the wick cannot overcome the sum of the liquid and vapor pressure drops which results in dry-out.

2) Vapor Pressure Limit

It is also called viscous limit and it occurs at low temperatures, where the pressure is very small and the viscous forces may overcome the inertial forces and limits the fluid circulation.

3) Sonic Limit

Vapor flow from the evaporator to the condenser section of a heat pipe is similar to a converging-diverging nozzle with a constant mass flow rate. Along the evaporator section, the velocity of the vapor increases and at the exit of this section reaches a maximum. If this maximum velocity at the end of the evaporator exceed the speed of sound, the choked flow condition will happen which is called the sonic limitation.

4) Entrainment Limit

Since the liquid and the vapor move in opposite direction, the vapor applies a shear force on the liquid at their interface. This shear force may overcome the surface tension of the liquid at high relative velocities and some droplets of liquid can be entrained into the vapor flow and results in a dry-out in evaporator section.

5) Boiling Limit

High heat flux applied to the evaporator section may result in nucleate boiling in wick structure. The vapor bubbles created in the liquid layer can block the pores and decrease vapor flow and limit the rate of heat conduction from the heat pipe wall to the liquid.

2.2 Literature Review

A review of vapor chambers and heat pipes analytical, numerical and experimental modeling approaches will be present in this section.

2.2.1 Analytical Modeling Approaches

A number of analytical models with approximation have been proposed to investigate the thermal performance of heat pipes and vapor chambers.

A thermal resistance network model was presented to predict steady state performance of heat pipes and vapor chambers [9]. The model was represented by multiple solid components with specific thermal resistances. Details of the calculation of thermal resistances were presented. The model does not capture the working fluid behavior and only addresses the steady state performance. This work was extended to develop a model to analyze transient performance of heat pipes [10]. Transient governing equation for each component was simplified to a first order differential equation. The fluid behavior in the heat pipe was considered as a thermodynamics cycle. The phase change process in this model is assumed to occur with negligible temperature change. Therefore, conduction in the walls and the wick dominated the convective effect of the fluid. The results were compared with experimental and numerical models.

A simple conduction based model for vapor chamber of both remote and active cooling mode was developed in [11]. Effective thermal conductivity of the vapor core was derived using ideal gas law and Clapeyron equation. The model was compared with experiments and showed a good agreement. While this model is only capable of analyzing steady state performance and does not account for fluid flow inside the vapor chamber, it provides designers with a simple model that can be used to compare heat pipes and vapor chambers performance with traditional solid metal heat spreaders.

Performance of a vapor chamber was investigated for both uniform and non-uniform heating conditions experimentally. The results showed that performance of the vapor chamber is not sensitive to non-uniform heat conduction [12]. Also an analytical model was developed to account for the effect of heat flux on the distribution of the working fluid in the sintered particle wick. The model uses statistical analysis to predict the fraction of the saturated pores for different amounts of heat flux.

Thermal performance of a heat pipe integrated with a heat sink was investigated in [13]. Thermal resistances in the heat pipe were estimated. Effects of different variables on the thermal resistance of the heat pipes were studied.

An integral method was used to solve steady state non-dimensional governing equation for pseudo-three dimensional incompressible vapor flow in an asymmetrical flat heat pipe [14]. Temperature and pressure distribution of the vapor inside the heat pipe were evaluated. This study was extended to investigate transient analysis of heat pipes during startup and shut down operations. [15,16].

An analytical model was developed to investigate the transient behavior of flat plate and disk shaped heat pipes during startup operation [15]. A transient heat conduction model was employed to describe heat transfer in the wall and the wick structure. Transient behavior of the vapor core was represented by a pseudo-three dimensional approximation. The two models then coupled with each at the liquid-vapor interface other to develop a complete model of the heat pipe. The model was solved for temperature, velocity and pressure using an integral method.

Mathematical transient models were developed for both startup and shut down operations of a flat plate heat pipe [16]. Results showed that the heat pipe time constants depend on the heat input and the thermal and physical properties of the wall and the wick such as thermal diffusivity and thickness. Results also revealed that the dominant

resistance in the heat pipe is due to the wick structure. The results of this study were compared to the experimental investigation of the same device [17,18] and showed a good agreement.

A three-dimensional heat conduction model in the wall was coupled with a two-dimensional hydrodynamic model for the liquid and vapor flows to formulate a steady state model of a flat micro heat pipe [17]. The model is capable of prediction the maximum heat transfer capability for a heat pipe with several electronic components.

Mass, momentum and energy equations were solved for a two-dimensional model of a vapor chamber including the wall, wick and vapor space [18]. Temperature in the wall and vapor pressure, velocity and temperature distribution were reported. Results indicated that the assumption that phase change takes place uniformly in the axial direction is valid only if the wall conduction is negligible in that direction. Also, the effects of the wall thermal conductivity, heat input and size of the heat source on the thermal performance of the vapor chamber were studied.

2.2.2 Numerical Modeling Approaches

A heat conduction-based thermal model of a vapor chamber cooling a single heat source was developed in [19]. The vapor chamber was modeled as multiple components with effective thermal conductivities. Effective thermal conductivities of the wick structure and vapor space were evaluated. Effects of the thermal conductivity of the wick and vapor space on the thermal performance of the vapor chamber were investigated. Results indicated that the performance of the vapor chamber is much more sensitive to effective thermal conductivity of the wick structure that the vapor space.

Three-dimensional vapor flow inside vapor space and the flow of the working fluid in porous domain in a vapor chamber were investigated using a numerical method [20]. A finite element approach based on Galerkin weighted residuals method was used

to solve the mass, momentum and energy equations. This study was an extension of a previous analytical work [15]. The numerical results were compared with the analytical solution and showed a good agreement.

A numerical procedure is developed to analyze thermal and mechanical performance of a vapor chamber [21]. Two dimensional continuity, momentum and energy equations were solved for the vapor and wick domains. Heat conduction equations were used to model heat transfer in the wall. A Brinkman-Forchheimer extended Darcy model is used to describe the fluid flow in the wick structure. Also, a finite element mechanical model is developed to investigate the effect of the vapor chamber on die stresses. The results showed that a vapor chamber not only can perform better than copper spreaders in thermal point of view, but also will reduce the stress in the chip.

A numerical study was conducted to analyze the effect of vapor pressure drop on the performance of a cylindrical heat pipe [22]. Governing equations were solved using a finite difference iterative method. Results showed that the variation of the vapor pressure can affect the performance of the heat pipe significantly.

A two dimensional compressible laminar model was developed to investigate the steady state and transient behavior of a flat heat pipe [23]. The simple algorithm was employed to solve the governing equations. Results showed that different variables such as the working fluid, geometry and heat flux rate can affect the vapor transient time.

A numerical model is developed to investigate the transient performance of flat heat pipes [24]. Two dimensional governing equations in the wick and vapor regions were discretized and solved using the SIMPLE algorithm. System pressure, temperature and velocity fields were computed. A parametric study on heat input and vapor core thickness showed the total pressure drop at the liquid-vapor interface decreases by increasing vapor region thickness.

A two dimensional numerical finite volume analysis was employed to find the temperature profile across a vapor chamber next to a local heat source [25]. A simplified transient three-dimensional model which considers vapor as a common interface between evaporator and condenser wicks was proposed to determine the temperature distribution in a vapor chamber [26]. This model was used to simulate a heat sink embedded with a vapor chamber [27].

2.2.3 Experimental Modeling Approaches

Thermal performance of a vapor chamber was investigated experimentally in [28]. Results showed the main thermal resistance in the vapor chamber is due to the wick structure. The performance of the vapor chamber was compared with copper and aluminum heat spreaders and the results indicated that the performance of the vapor chamber and copper block are close to each other. Vapor chambers are found to outperform copper heat sinks for applications with large footprint area.

Performance of a vapor chamber charged with acetone, water and methanol as working fluids were determined experimentally and compared with each other [29]. Results showed that water presents the minimum vapor chamber resistance and maximum heat loads and the minimum heat loads and maximum resistance were obtained from acetone.

In a series of studies, thermal resistance of a vapor chamber, effect of heat source size and heat generation rate on the vapor chamber thermal resistance were investigated experimentally [30,31]. Results showed that the thermal resistance of the vapor chamber increases when the heat source size decreases and is not sensitive to the amount of heat flux.

Thermal performance of a flat heat pipe was carried out experimentally in [32]. Results indicated that the main thermal resistance of the heat pipe is due to the wick in

the evaporator section. Temperature difference between evaporator and condenser side was found to be small. Effect of input heat flux and heat transfer coefficient on the thermal performance of a flat plate heat pipe during startup and shut down operation was investigated experimentally [33]. Results showed that the heat transfer coefficient has a strong effect on the heat pipe transient time and small effect on the maximum temperature difference. In contrast, heat flux rate has a significant role on the temperature rise and less effect on the heat pipe transient time.

Chapter 3

Pure Conduction Model

In this chapter, first, a simplified pure conduction model is developed for a vapor chamber integrated with a single heat source. Vapor chamber components are modeled as multiple layers of solids with effective thermal conductivities. Details of evaluating effective thermal conductivity for vapor chamber components are presented. Next, the model is extended for a system of multiple low power chips. Thermal performance of the vapor chamber for single chip scenario is compared to the multiple chips scenario. Emphasis is on the impact of using multiple lower power chips instead of a single high power chip on the heat spreading capability of a flat, thin, vapor chamber. In the last section, the effect of copper wall thickness on the performance of the vapor chamber will be investigated.

3.1 Vapor Chamber Model for Single Heat Source

3.1.1 Geometry

Figure 3-1 shows a schematic of the vapor chamber geometry introduced in this section. The length and the width of the vapor chamber are 50×50 mm with the total height of 2.4 mm. The lower and upper walls are made of copper and the working fluid is water. The porosity and permeability of the wick are assumed to be 0.5 and 1.43×10^{-11} m^2 respectively [24]. The chip attached on the bottom of the vapor chamber is made of silicon and the dimensions are 10×10×0.7 mm. The origin of the coordinate system is placed at the center of the bottom surface of the chip.

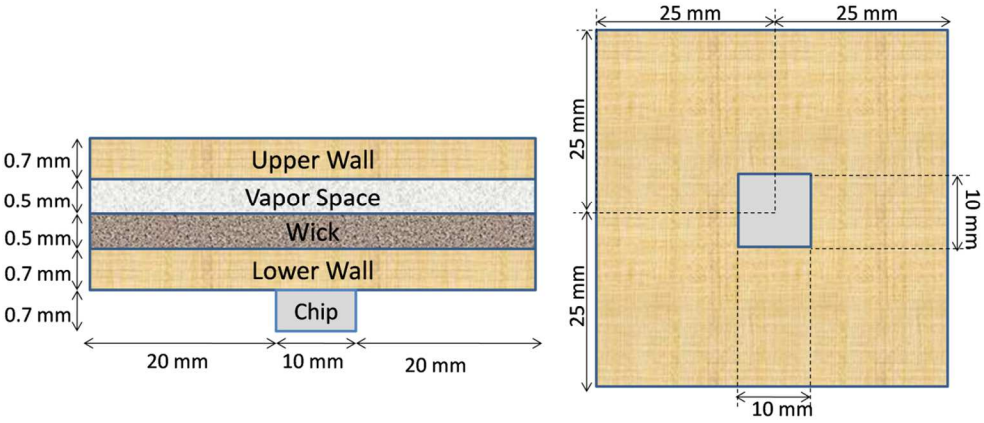

Figure 3-1: Schematic of the Geometry of the Vapor chamber

3.1.2 Boundary Conditions

Heat is applied on the bottom surface of the chip and the top surface of the upper wall is cooling down with the ambient temperature. Heat transfer coefficient on the condenser side is 885 W/m^2-K and the ambient temperature is considered to be 35 °C. All other boundary conditions are adiabatic.

3.1.3 Effective Thermal Conductivities of Vapor Chamber Components

Next step is to define the thermal conductivity for different parts of the vapor chamber. Thermal conductivities of silicon chip and copper walls are known values. Since wick structure and vapor space are modeled as solid layers, we need to define the value of effective thermal conductivity for them.

a) Effective Thermal Conductivity of the Wick Structure

There are several methods presented in literature to calculate the effective thermal conductivity for wick structures such as parallel, serial and sintered assumption. All of these methods use the thermal conductivities of the copper and the water along with the porosity of the wick to evaluate the thermal conductivity of the wick structure [34,35].

a) Parallel Assumption

$$k_w = (1-\varepsilon)k_s + \varepsilon k_l \tag{3.1}$$

b) Series Assumption

$$k_w = (1-\varepsilon)k_s + \varepsilon k_l \tag{3.2}$$

c) Sintered Wick Structure

$$k_w = \frac{\pi}{8}\left(\frac{r_c}{r_s}\right)^2 k_s + \left[1 - \frac{\pi}{8}\left(\frac{r_c}{r_s}\right)^2\right]\left[\frac{k_l k_s}{\varepsilon' k_s + k_l(1-\varepsilon')}\right] \tag{3.3}$$

Where

$$\varepsilon' = \frac{\varepsilon}{\frac{\pi}{8}\left(\frac{r_c}{r_s}\right)} \tag{3.4}$$

Where k_l and k_s are the thermal conductivities for the liquid and solid part, r_c and r_s are the contact radius and the particle sphere radius respectively, and epsilon is the porosity of the wick.

In this study, the equation (3.3) for sintered wick structure is used. The typical value evaluated from equation (3.13) in literatures is around 30-40 W/m-K. In this study, thermal conductivity of the wick structure is considered to be 40 W/m-k which is also used in [22,36].

b) Effective Thermal Conductivity of the Vapor Chamber

Prasher [6] used Clapeyron equation and ideal gas low to derive the effective thermal conductivity of the vapor space as a function of vapor space thickness and thermodynamic properties. The vapor was considered to be incompressible and the vapor flow was laminar and fully developed. The effective thermal conductivity of the vapor space can be calculated using equation (3.5).

$$\mathrm{k_v} = \frac{\mathrm{L^2 P_v \rho_v d^2}}{\mathrm{12 R \mu_v T^2}} \tag{3.5}$$

Where L is the latent heat of vaporization, d is the thickness of the vapor space, R is gas constant, T is temperature, P_v, μ_v, ρ_v, are pressure, viscosity and density of the vapor, respectively.

Wei and Sikka [19] used equation (3.5) to calculate the effective thermal conductivity for different temperature then used regression to present a correlation with new coefficients. As in shown in equation (3.6), this correlation is only a function of temperature and vapor space thickness which is more convenient to use.

$$k_v = C_0 \exp(a_0 T^2 + a_1 T + a_2) \left(\frac{d}{0.4}\right)^2 \quad (3.6)$$

Where C_0=0.165, a_0=-0.000349, a_1=0.124, a_2=6.756 and d is the thickness of the vapor space in mm.

They also investigated the effect of vapor space thermal conductivity on the performance of the vapor chamber. Results are shown in figure 3.2. It can be seen that for a large range of thermal conductivity of vapor space, the junction temperature does not change considerably. Therefore, it is safe to use a constant high number to represent the thermal conductivity of the vapor space. In this study, thermal conductivity of the vapor space is assumed to be 30000 W/m-K.

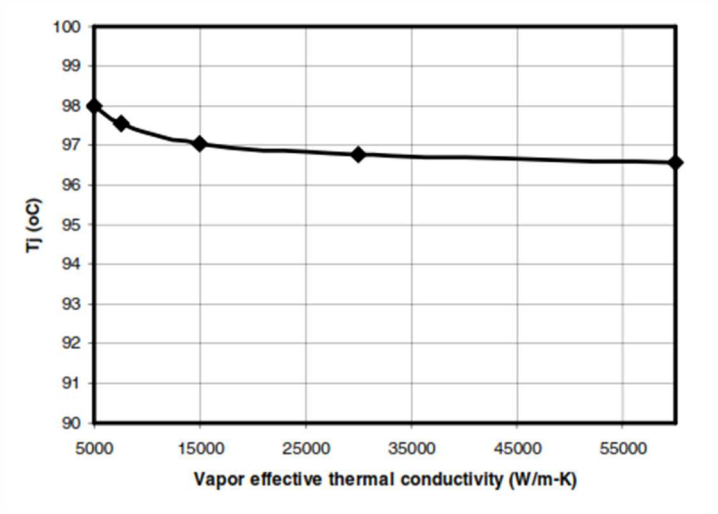

Figure 3-2: Effect of Vapor Thermal Conductivity on the Junction Temperature [19]

The geometry, boundary conditions and thermal conductivities of the vapor chamber components have been defined completely. Table 3.1 shows the values for dimensions and thermal conductivities of vapor chamber components.

Table 3-1: Thermal Conductivity and Dimensions of Vapor Chamber Components

Parts	Dimensions	Thermal Conductivity (W/m-K)	Material
Chip	10x10x0.7	117	Silicon
Lower Wall	50x50x0.7	385	Copper
Wick	50x50x0.5	40	Sintered Cu Powder
Vapor Space	50x50x0.5	30000	Water vapor
Upper Wall	50x50x0.7	385	Copper

3.1.4 Steady State Analysis

Since the problem is pure conduction, the three dimensional steady state governing energy equation can be written as equation (3.7).

$$\frac{\partial^2 T}{\partial x^2} + \frac{\partial^2 T}{\partial y^2} + \frac{\partial^2 T}{\partial z^2} = 0 \tag{3.7}$$

Equation (3.7) can be written separately for the chip and the vapor chamber and connected to each other using the conservation of energy at their interface. The governing energy equation and all boundary conditions for the chip and the vapor chamber are summarized below.

a) Chip

$$\frac{\partial^2 \mathrm{T_c}}{\partial x^2} + \frac{\partial^2 \mathrm{T_c}}{\partial y^2} + \frac{\partial^2 \mathrm{T_c}}{\partial z^2} = 0 \tag{3.8}$$

Subjected to the following boundary conditions

$$\frac{\partial \mathrm{T_c}}{\partial x} = 0 \qquad x = -5, x = 5 \tag{3.9}$$

$$\frac{\partial \mathrm{T_c}}{\partial y} = 0 \qquad y = -5, y = 5 \tag{3.10}$$

$$k_{si}\frac{\partial \mathrm{T_c}}{\partial z} = 100\, {}^{W}/_{cm^2} \qquad z = 0 \tag{3.11}$$

$$-k_{si}\frac{\partial T_c}{\partial z} = q'' \qquad z = 0.7 \tag{3.12}$$

Where subscript c and Si stands for chip and silicon, and q" is the heat flux at the interface between the chip and the vapor chamber which is unknown. The dimension values written above are in mm.

b) Vapor Chamber

$$\frac{\partial^2 \mathrm{T_v}}{\partial x^2} + \frac{\partial^2 \mathrm{T_v}}{\partial y^2} + \frac{\partial^2 \mathrm{T_v}}{\partial z^2} = 0 \tag{3.13}$$

Subjected to the following boundary conditions:

$$\frac{\partial T_v}{\partial x} = 0 \qquad x = -25, x = 25 \tag{3.14}$$

$$\frac{\partial T_v}{\partial y} = 0 \qquad y = -25, y = 25 \tag{3.15}$$

$$-k_{Cu}\frac{\partial T_v}{\partial z} = Q'' \qquad z = 0.7 \tag{3.16}$$

$$-k_{Cu}\frac{\partial T_v}{\partial z} = h(T - T_\infty) \qquad z = 3.1 \tag{3.17}$$

Where:

$$Q'' = \begin{cases} q'' & , -5 \le x \le 5, -5 \le y \le 5 \\ 0 & , Otherwise \end{cases} \tag{3.18}$$

A finite element simulation tool is used to solve the governing energy equation and find the temperature distribution in the vapor chamber. The entire geometry and all the boundary conditions are defined in ANSYS. The heat applied at the bottom surface of the chip is considered to be uniform. The cooling phenomenon is modeled by assigning a convective heat transfer coefficient on the top boundary, resembling a heat sink solution. Figure 3-3 shows the final mesh structure for the vapor chamber geometry which contains 859K elements. Since the number of elements in the mesh determines the accuracy of the results, the simulation is repeated at greater number of nodes and the mesh is refined until the results are grid independent.

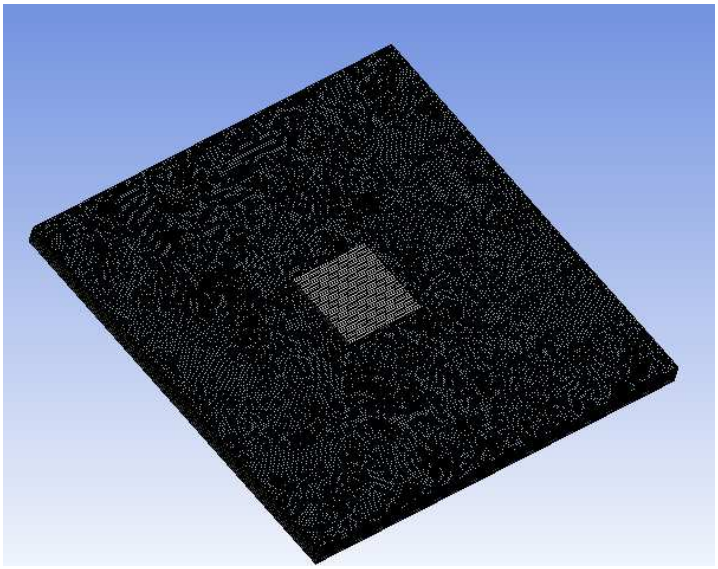

Figure 3-3: Mesh Structure for 859K Elements

By doing all the steps mentioned above, a steady state thermal simulation model is developed. Temperature distribution within the vapor chamber and the chip regions are shown in figure 3.4.

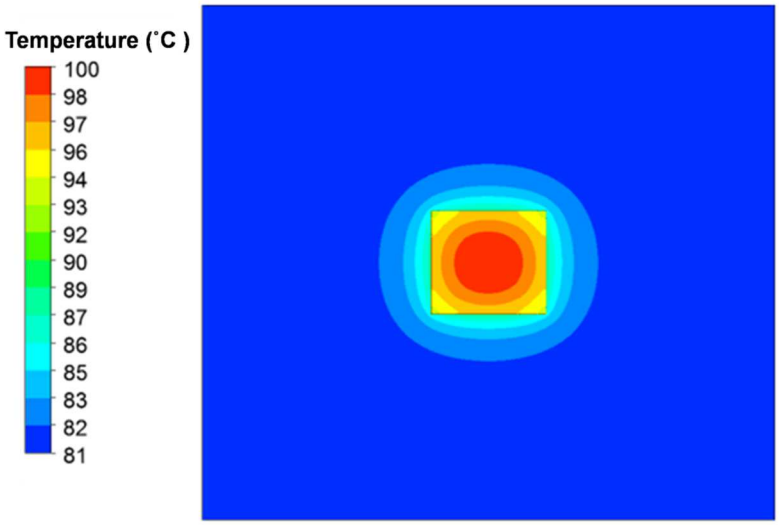

Figure 3-4: Temperature Distribution in Vapor Chamber (Bottom View)

As it is seen, the hot spot is the center of the chip bottom wall with the maximum temperature equal to 100 °C. Figure 3-5 shows the temperature distribution for the vapor chamber from another view.

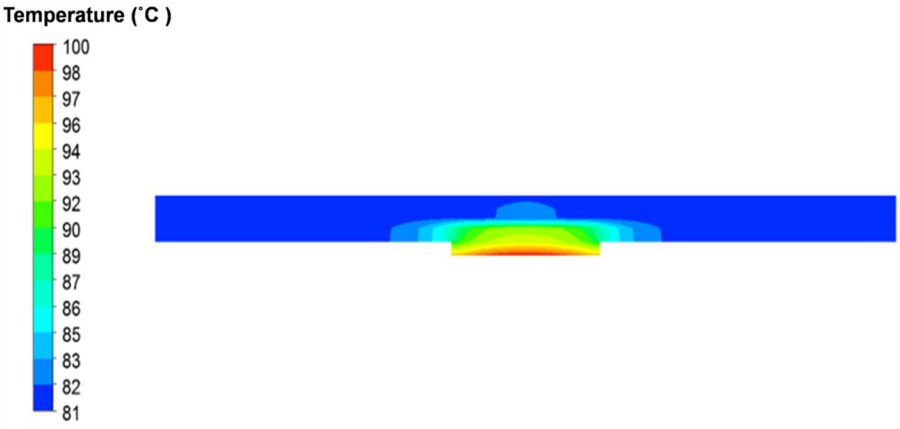

Figure 3-5: Temperature Distribution in Vapor Chamber (Front View)

A plot of the temperature profile for different components of the vapor chamber will help to have a better understanding of the thermal resistance of these components. Figure 3-6 shows a plot of temperature along the center lines for vapor chamber components. It is shown that there is a significant temperature drop from the wick to the vapor space which indicates that the dominant resistance is due to the wick structure. It is also seen that the temperature profile is more uniform at the vapor space and upper wall.

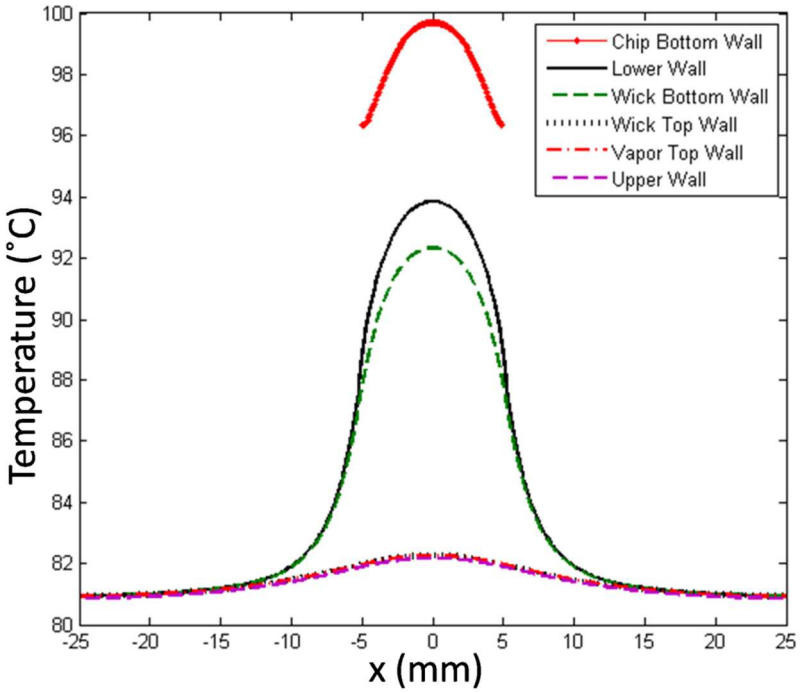

Figure 3-6: Temperature Distribution along the Center Lines for Vapor Chamber Components

3.2 Vapor Chamber Model for Multiple Heat Sources

In this section, emphasis is on the impact of using multiple lower power chips instead of a single high power chip on the heat spreading capability of a flat, thin, vapor chamber. The same vapor chamber analyzed in the previous section is used for modeling a multiple heat-source scenario. Instead of one single chip, three lower power chips are considered in this model.

3.2.1 Model Description

Figure 3.7 shows a schematic of the geometry of the vapor chamber integrated with multiple chips. The same vapor chamber is attached to three chips of equal dimension, each being the same as the single heat-source considered in the previous section. The chips are assumed to be aligned to each other. The heat flux on the bottom

surface of the chips from left to right is assumed to be 25 W/cm^2, 50 W/cm^2 and 25 W/cm^2 respectively, making the total heat dissipated equivalent to the single chip scenario. All other boundary conditions are the same as the previous simulation.

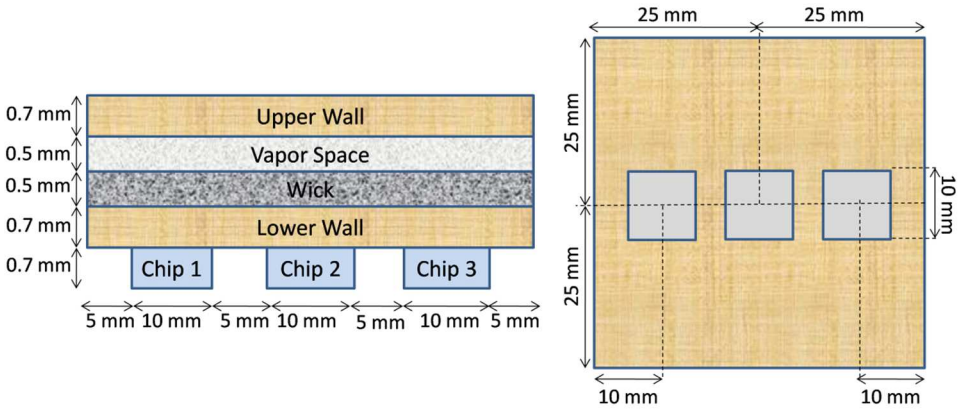

Figure 3-7: Schematic of the Geometry of the Vapor Chamber

3.2.2 Steady State Analysis

The new geometry of the vapor chamber is defined and meshed in ANSYS and all the boundary conditions are applied. Figure 3-8 and 3-9 show the contour plots of the temperature profile in the vapor chamber for three chips case from bottom and front views, respectively. It is seen that the maximum temperature is lower in this case compared with single high power chip model due to better heat spreading across the base of the vapor chamber.

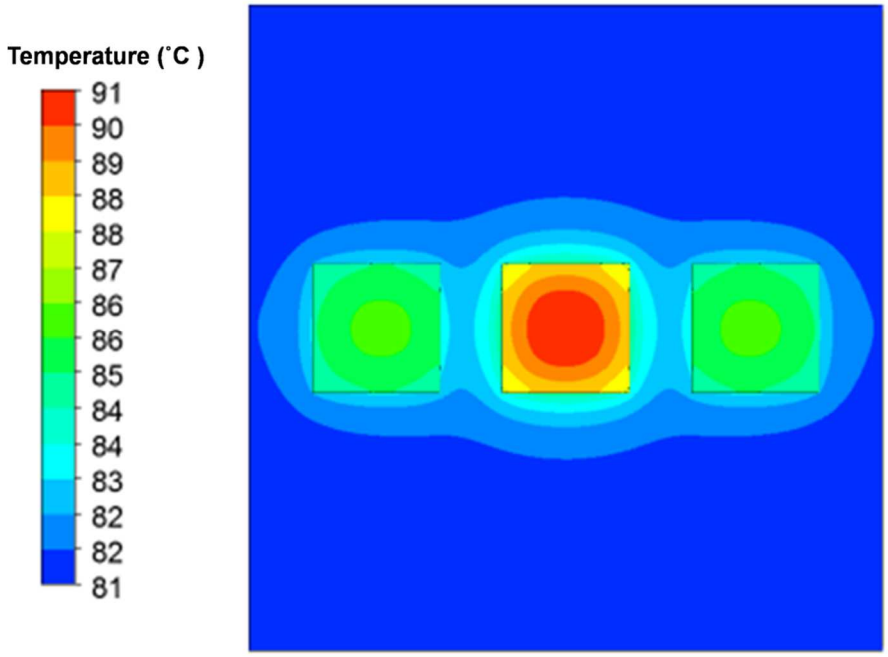

Figure 3-8: Temperature Distribution in Vapor Chamber (Bottom View)

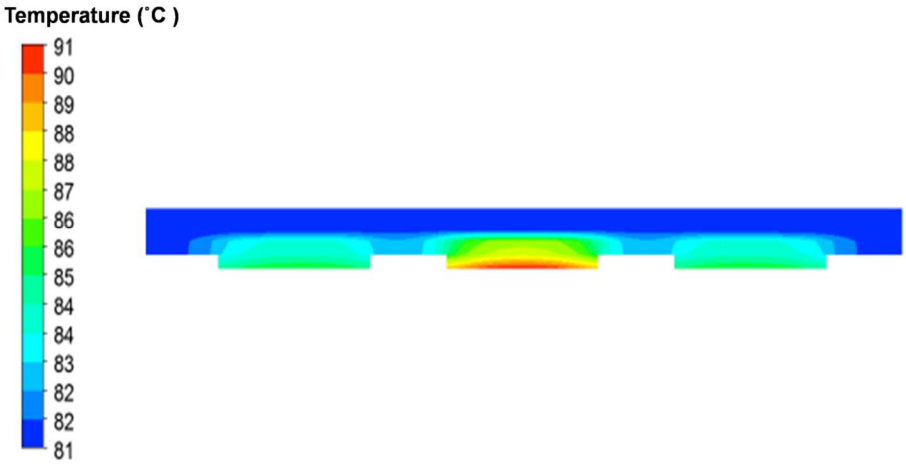

Figure 3-9: Temperature Distribution in Vapor Chamber (Front View)

The plot of temperature profile along the center line for vapor chamber components is shown in figure 3-10.

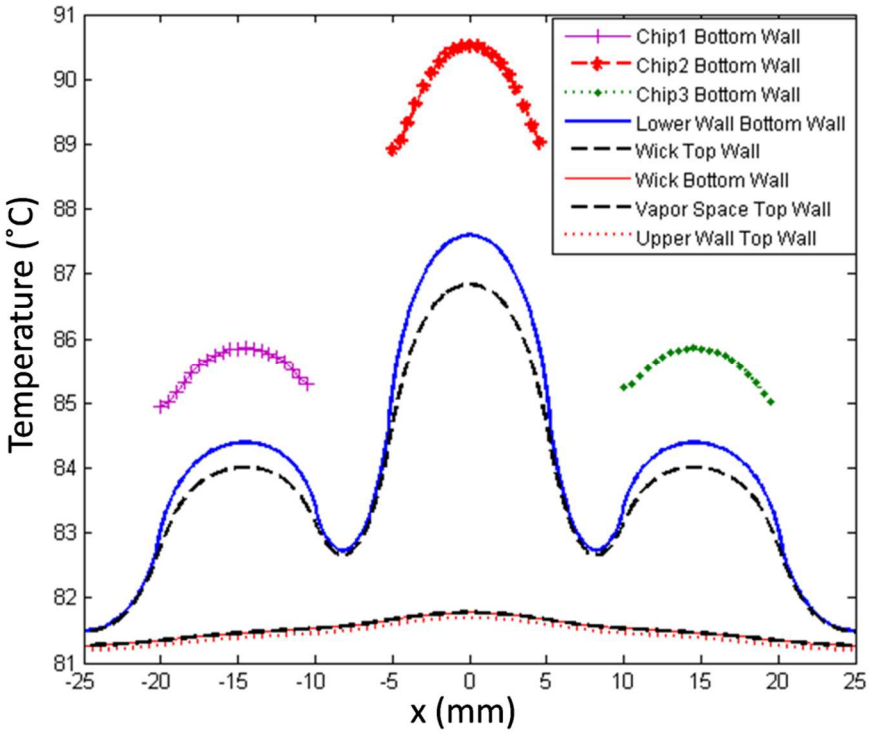

Figure 3-10: Temperature Distribution along the Center Lines for Vapor Chamber Components

3.2.3 Effect of Using Multiple Chips on the Performance of Vapor Chamber

A comparison between the temperature distribution in the vapor chamber for single and multiple chips scenarios is shown in figure 3-11. Same temperature range is used to produce temperature contours for both scenarios so the difference between the colors of the contours clearly shows the temperature difference between two cases. It is seen that the maximum temperature in multiple chip scenario is 91˚C as opposed to 100˚C in single chip scenario due to better heat spreading across the base of the vapor chamber. Therefore, using a system of multiple low power chips instead of a single high power chip improves thermal performance of the vapor chamber considerably.

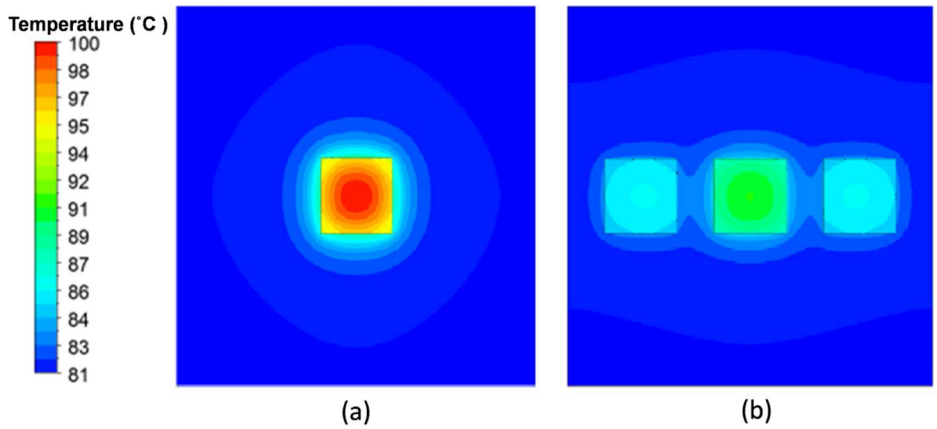

Figure 3-11: Steady State Temperature Distribution for (a) Single Chip and (b) Multiple Chips

Simulation results show that by integrating the same vapor chamber with multiple low power chips instead of one high power chip, the maximum junction temperature of chip decreases despite the same total power generation. Therefore, the performance of the vapor chamber can be improved by distributing the power of a single chip into multiple chips. This result indicates that if it is needed to maintain the junction temperature at a desired value such as 100 ˚C assuming same heat transfer coefficient and total heat flux as the single-chip scenario, due to the reduction in junction temperature in multi-chip scenario, one can design a vapor chamber with thinner vapor space or copper walls to meet the desirable T_j. In other words, these results indicate a possibility for designing the vapor chamber in such a way that the material usage and costs are reduced. The effect of copper wall thickness on the performance of the vapor chamber will be investigated in next section.

3.2.4 Effect of copper wall thickness on vapor chamber performance

In this section, the simulation for the multiple chip vapor chamber is repeated for different values of copper wall thickness. Temperature profile of the three chips for different values of copper wall thickness is shown in figure 3-12. Figure 3-13 shows the maximum junction temperature and also the mass of vapor chamber for different values of copper wall total thickness.

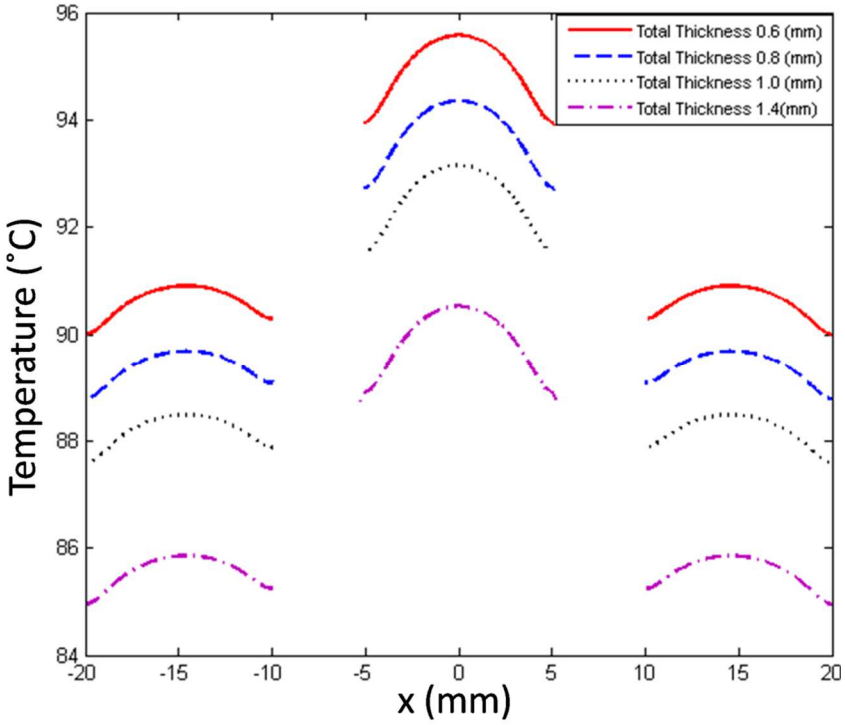

Figure 3-12: Chips Temperature Profile for Different Total Thickness of Copper Walls

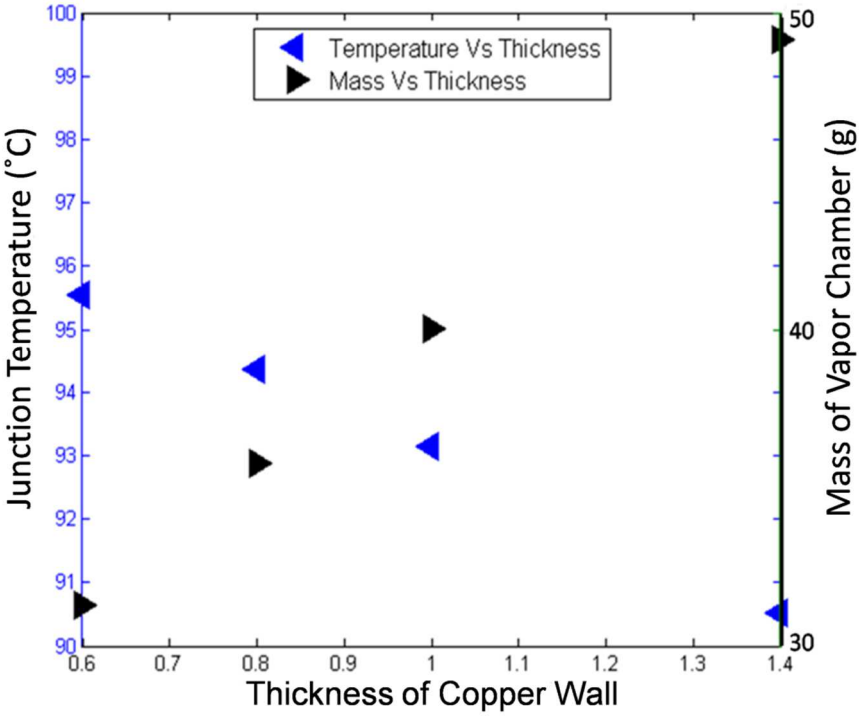

Figure 3-13: Junction Temperature and Mass of Vapor Chamber for Different Total Thickness of Copper Walls

These results indicate that using a system of multiple low power chips instead of a single chip improves the thermal performance of the vapor chamber, and provides designers with the opportunity for designing vapor chamber with same functionality at reduced mass. However, it is important to analyze the effect of incorporating multiple low power chips on overall cost, since this approach may lead to increased design and process complexity. Based on a trade-off between cost and thermal performance, it is possible that vapor chambers with multiple low power chips may be relevant for a variety of applications in semiconductor packaging.

Chapter 4

Multi-Physics Model

In previous chapter, a simplified pure conduction model of a vapor chamber was developed. Since vapor chamber components were modeled simply as solids with effective thermal conductivities, the model does not capture fluid flow in the wick structure and vapor space. Another limitation of the previous model is that it only predicts steady state performance and does not provide any information about the temperature in different time intervals.

In this chapter, a simplified multi-physics model which is capable of accounting for fluid motion in wick structure will be presented. By inclusion of the fluid flow phenomena, it is expected that the model captures the vapor chamber dynamics more realistically. Steady state and transient numerical simulation of a vapor chamber for both single and multiple chips scenarios will be carried out. The performance of this model will be compared with the simplified conduction model. Vapor chamber performance for the increasingly common scenario of multiple chips is evaluated. Also, the effect of heat density and chip orientation on the performance of vapor chamber will be studied.

4.1 Multi-Physics Vapor Chamber Model

The operation of a vapor chamber consists of heat conduction in the walls, liquid flow in the wick structure, vapor flow inside the vapor space and the liquid and vapor flow interaction. The governing equations for each of these basic mechanisms will be discussed in the following section [24].

4.1.1 Governing Equations

1) Conduction in the Walls

The transient energy equation in the wall can be written as:

$$\rho_s C_s \frac{\partial T}{\partial t} = \nabla.(k_s \nabla T) \tag{4.1}$$

2) Liquid Flow in the Wick Structure

The continuity, momentum and energy equation for the liquid flow inside the wick structure can be written as:

$$\varphi \frac{\partial \rho_l}{\partial t} + \nabla.(\rho V)_l = 0 \tag{4.2}$$

$$\frac{\partial(\rho u)_l}{\partial t} + \nabla.(\rho V u)_l = g_x - \varphi \frac{\partial P_l}{\partial x} + \nabla.(\mu \nabla u)_l - \frac{\mu_l \varphi}{k_l} u_l - \frac{C_E \varphi}{k_l^{0.5}} (\rho |V| u)_l \tag{4.4}$$

$$\frac{\partial(\rho v)_l}{\partial t} + \nabla.(\rho V v)_l = g_y - \varphi \frac{\partial P_l}{\partial y} + \nabla.(\mu \nabla v)_l - \frac{\mu_l \varphi}{k_l} v_l - \frac{C_E \varphi}{k_l^{0.5}} (\rho |V| v)_l \tag{4.5}$$

$$\frac{\partial(\rho w)_l}{\partial t} + \nabla.(\rho V w)_l = g_z - \varphi \frac{\partial P_l}{\partial z} + \nabla.(\mu \nabla w)_l - \frac{\mu_l \varphi}{k_l} w_l - \frac{C_E \varphi}{k_l^{0.5}} (\rho |V| w)_l \tag{4.6}$$

$$(\rho C)_m \frac{\partial T}{\partial t} + \nabla.(\rho C V T)_l = \nabla.(k_{\text{eff}} \nabla T_l) \tag{4.7}$$

Where

$$(\rho C)_m = (1 - \varphi)(\rho C)_s + \varphi (\rho C)_l \tag{4.8}$$

The momentum equation for the fluid flow inside the wick is obtained from momentum equations for porous media.

3) Vapor Flow in the Vapor Space

The continuity, momentum and energy equation for the vapor flow inside the vapor core can be written as:

$$\frac{\partial \rho_v}{\partial t} + \nabla.(\rho V)_v = 0 \tag{4.9}$$

$$\frac{\partial(\rho u)_v}{\partial t} + \nabla.(\rho V u)_v = g_x - \frac{\partial P_v}{\partial x} + \nabla.(\mu \nabla u)_v \tag{4.10}$$

$$\frac{\partial(\rho v)_v}{\partial t} + \nabla.(\rho V v)_v = g_y - \frac{\partial P_v}{\partial y} + \nabla.(\mu \nabla v)_v \tag{4.11}$$

$$\frac{\partial(\rho w)_v}{\partial t} + \nabla.(\rho V w)_v = g_z - \frac{\partial P_v}{\partial z} + \nabla.(\mu \nabla w)_v \tag{4.12}$$

$$(\rho C)_v \frac{\partial T_v}{\partial t} + \nabla.(\rho C V T)_v = \nabla.(k_{\text{v}} \nabla T_v) \tag{4.13}$$

4) Liquid-Vapor Interface

If the phase change from liquid to vapor occurs at the interface of the wick structure and vapor space, the interface temperature can be calculated using the conservation of energy at the interface.

$$-k_w A_i \frac{\partial T}{\partial y} + m_i C_l T_i = -k_v A_i \frac{\partial T}{\partial y} + m_i C_v T_i + m_i h_{fg} \quad (4.14)$$

Where, m_i is the mass flux at the interface. Several studies provided different expressions based on either energy balance or kinetic theory to calculate the mass flux at the interface. Based on kinetic theory, the interface mass flux can be evaluated from equation (4.15).

$$m_i = \left(\frac{2\sigma}{2-\sigma}\right)\left(\frac{1}{2\pi R}\right)^{0.5}\left(\frac{P_v}{(T_v)^{0.5}} - \frac{P_i}{(T_i)^{0.5}}\right) \quad (4.15)$$

Where, P_i is the interface pressure and it can be calculated from the Clausius-Clapeyron equation.

$$\frac{R}{h_{fg}} \ln\left(\frac{P_i}{P_0}\right) = \frac{1}{T_0} - \frac{1}{T_i} \quad (4.16)$$

Where, P_i and T_i are the reference pressure and temperature, respectively.

The thermal-fluid phenomena occurring during the operation of a vapor chamber were shown mathematically in above equations. As it can be seen, velocity, pressure and temperature fields are highly dependent. The phase change occurs at the wick-vapor interface which is not a usual boundary condition in commercial simulation tools. Therefore, solving the governing equations and applying boundary conditions is a very complicated process which is usually results in expensive computational procedures. The purpose of this chapter is to develop a simpler model base on some assumptions with a fare accuracy which can be analyzed with available commercial simulation tools. In real applications, to reduce the complexity of the problem, some parts may be combined with

other regions, decoupled from other parts or neglected. The model description is presented in next section.

4.1.2 Model Description

The dimensions and geometry of the vapor chamber is considered to be same as the previous chapter. Fluid flow inside the wick structure will be taken into account in this model. Therefore, the solid layer which represented the wick structure in the previous model will be replaced by a porous domain consists of a thin layer of sintered copper saturated in water. For simplicity and avoiding the complication due to phase change, the vapor space is kept as a solid layer with effective thermal conductivity and the focus will be on the fluid flow inside the wick structure in this model.

Vapor chamber models are developed for both single and multiples chips cases. Heat is applied on the bottom surface of the chips, resembling the silicon active region, and the top surface of the upper wall is cooled by a heat sink at the ambient temperature. Heat transfer coefficient on the condenser side is set to 885 W/m^2-K and the ambient temperature is considered to be 35 ^oC. All other boundaries are adiabatic. In single heat source scenario, the heat applied on the chip is 100 W/cm^2. In multiple chips scenario, the chips are assumed to be aligned to each other and the heat fluxes on the bottom surface of the chips from left to right are assumed to be 25, 50 and 25 W/cm^2, respectively.

The reference pressure in the wick structure is considered to be 1 atm. The model is buoyant and the gravity is applied on z direction. The fluid flow is considered to be incompressible and laminar. Wick porosity and permeability is considered to be 0.5 and $1.43\times10^{-11}m^2$ respectively [24].

Vapor chamber geometry and all the boundary conditions are defined in ANSYS. ANSYS CFX is used as the solver. CFX uses finite volume method in which the mass, momentum and energy equations are conserved around the mesh elements.

4.1.3 Steady State Analysis

By updating the model, a steady state thermal and fluid simulation of the vapor chamber is developed. Contour plots of temperature distribution for both single and multiple chips cases are shown in figures 4-1. The maximum temperature in multi-chip scenario is 90˚C as opposed to 100˚C in single chip scenario. As expected, using a system of multiple low power chips instead of a single high power chip improves thermal performance considerably. Figure 4.2 shows the velocity profile of the working fluid inside the wick structure.

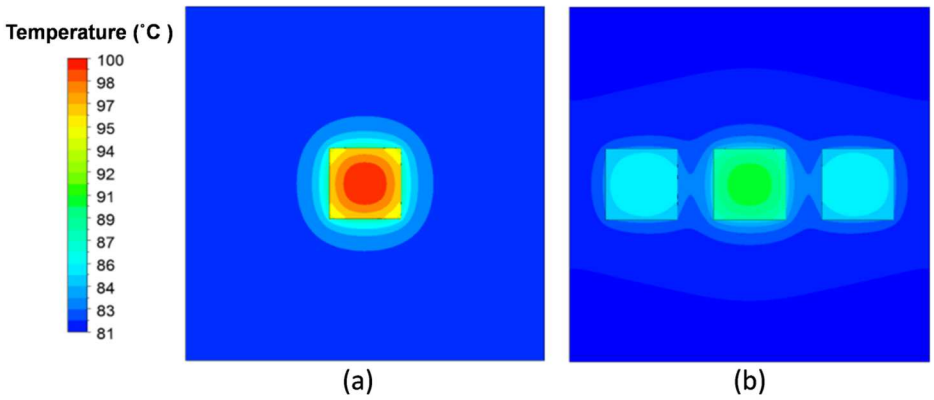

Figure 4-1: Steady State Temperature Distribution for (a) Single Chip and (b) Multiple Chips

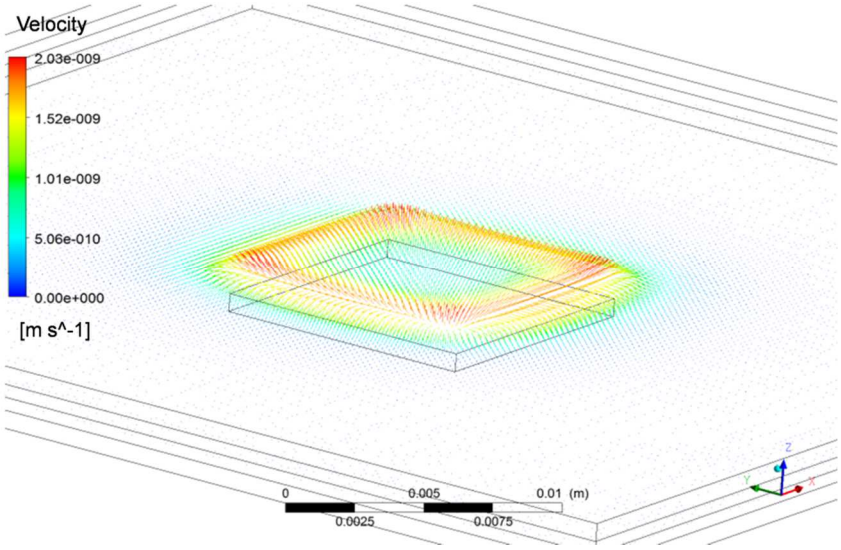

Figure 4-2: Velocity Profile of the Working Fluid inside the Wick Structure

(Single Chip Scenario)

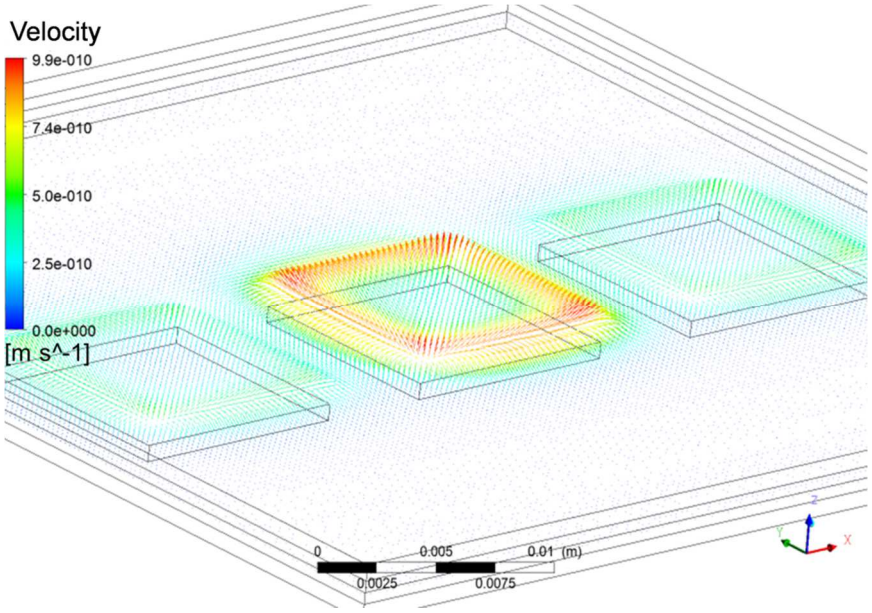

Figure 4-3: Velocity Profile of the Working Fluid inside the Wick Structure

(Multiple Chip Scenario)

4.1.4 Comparison with Pure Conduction Model

In this section, thermal performance of the simplified pure heat conduction model which was introduced in the previous chapter will be compared with the multi-physics model. Temperature profile of single and multiple chips for pure conduction and multi-physics models are shown in figure 4-4 and 4-5. It is seen that there is a good agreement between the two models. While both models can predict the thermal performance of the vapor chamber, the multi-physics model has the advantage of accounting for fluid flow inside the wick structure.

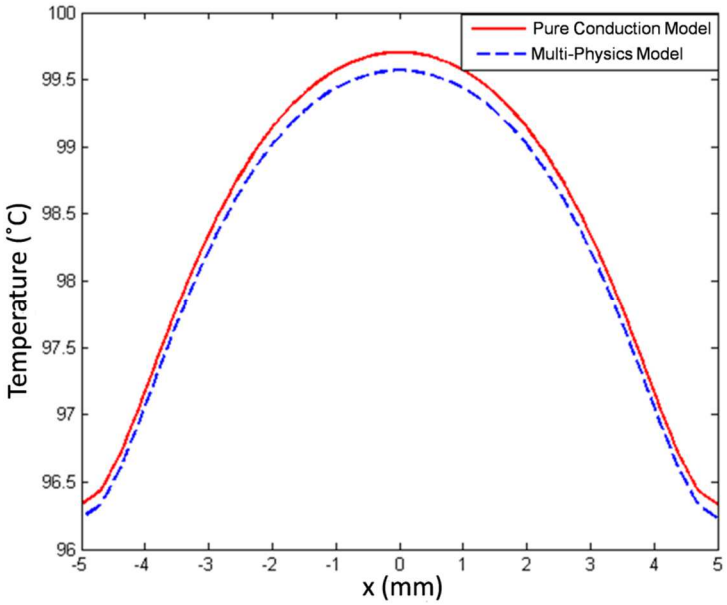

Figure 4-4: Chip Temperature Profile for Pure Conduction and Multi-Physics Model (Single Chip Scenario)

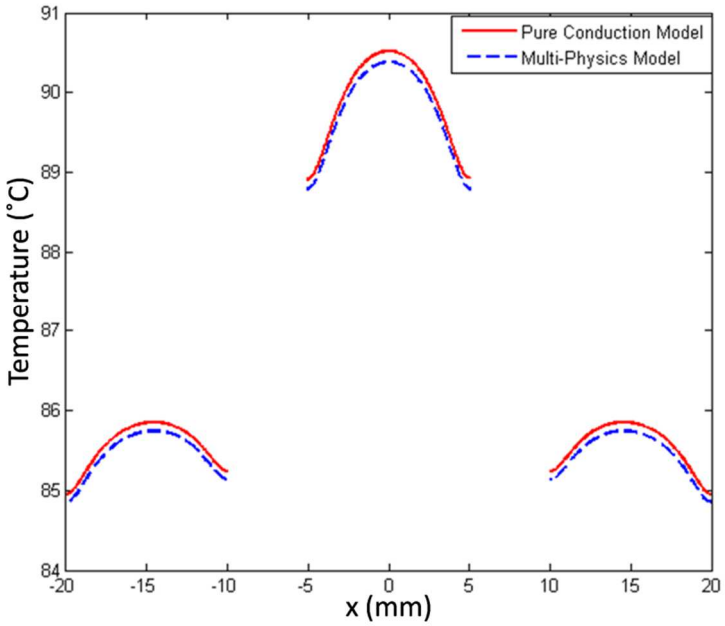

Figure 4-5: Chip Temperature Profile for Pure Conduction and Multi-Physics Model (Single Chip Scenario)

4.2 Model Validation

In this section, the multi-physics model presented in this study will be compared with the conduction model introduced by Wei and Sikka [19]. Wei and Sikka [19] investigated a 40.5x40.5 mm vapor chamber integrated with a chip of size 10x10 mm shown in figure 4-6. Chip is attached to the bottom surface of the vapor chamber using a thermal interface material (TIM) and the whole package is installed on a ceramic carrier with an insulating material. The carrier is not considered in the model presented here. Details of dimensions and thermal conductivities of the package components are presented in Table 4-2.

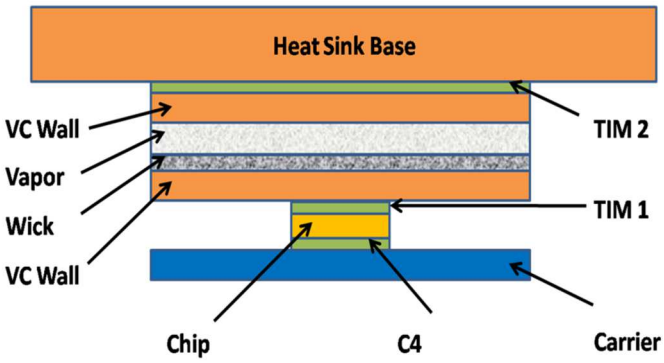

Figure 4-6: Schematic of the Vapor Chamber [19]

Heat flux applied at the bottom surface of the chip is 100 W/cm^2. Heat transfer coefficient assigned on the top surface of the heat sink base is 1400 W/K-m^2 and the ambient temperature is considered to be 35˚C. All other boundary conditions are adiabatic. The multi-physics model presented in previous sections is developed for the vapor chamber shown in figure 4-12.

Table 4-1: Dimensions and Thermal Conductivities [19]

Parts	Dimensions	Thermal Conductivity (W/m-K)	Material
Chip	10x10x0.785	117	Silicon
TIM 1	10x10x0.114	3.8	Thermal Paste
Lower Wall	40.5x40.5x1.5	385	Copper
Wick	40.5x40.5x0.5	30	Sintered Cu Powder
Vapor Space	40.5x40.5x1.0	30000	Water vapor
Upper Wall	40.5x40.5x1.0	385	Copper
TIM 2	40.5x40.5x0.1	3.8	Thermal Paste
Heat Sink Base	90x90x4	385	Copper

A comparison between temperature distribution for vapor chamber components from this study and the conduction model provided by Wei and Sikka [19] is shown in figure 4-7. Results show a good agreement between the multi-physics model presented in this study and the conduction model introduced in [19]. The contour plots of temperature distribution and velocity profile in the wick structure are shown in figure 4-8 and 4-9.

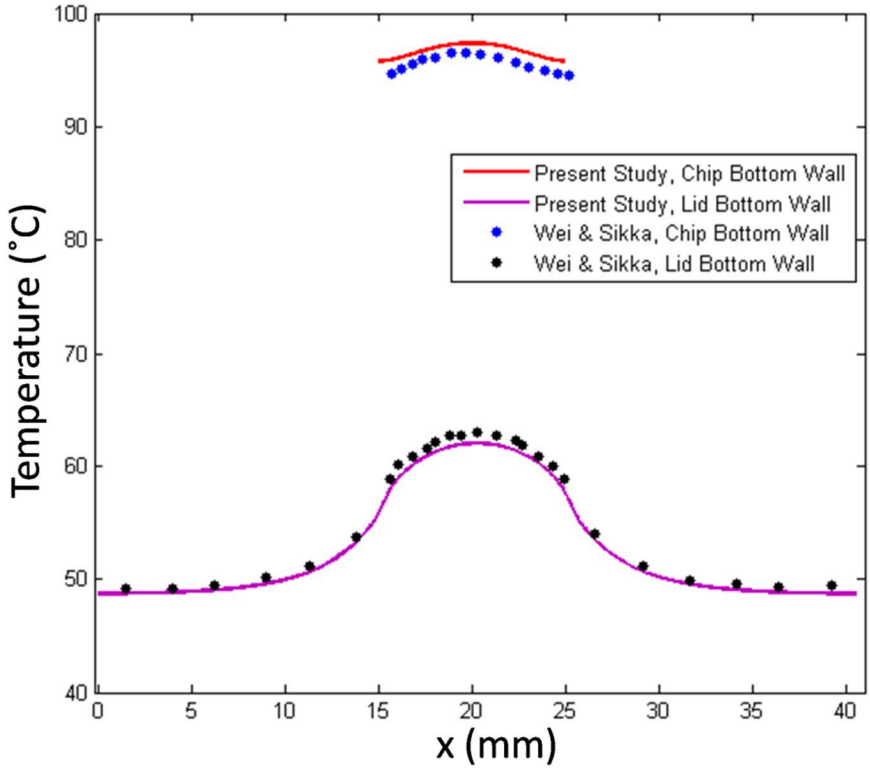

Figure 4-7: Chip and Wall Temperature Distribution for the Present Study and Conduction Model by Wei and Sikka

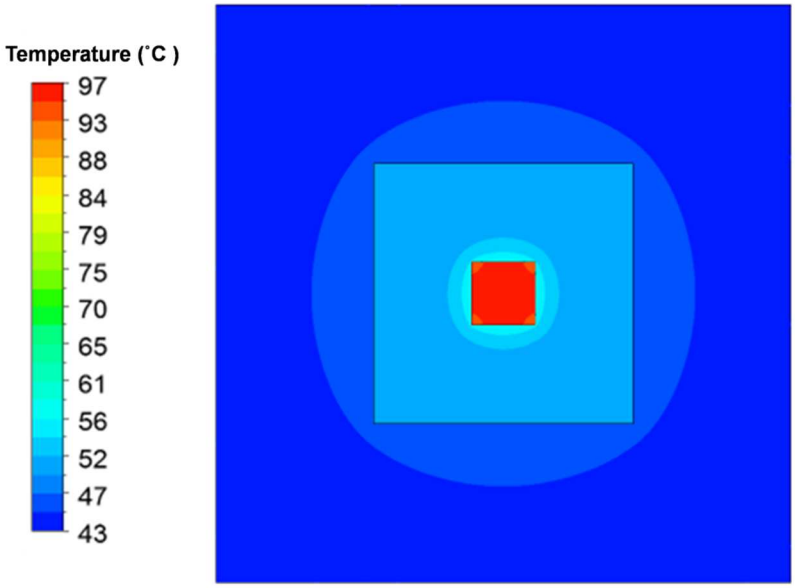

Figure 4-8: Temperature Distribution

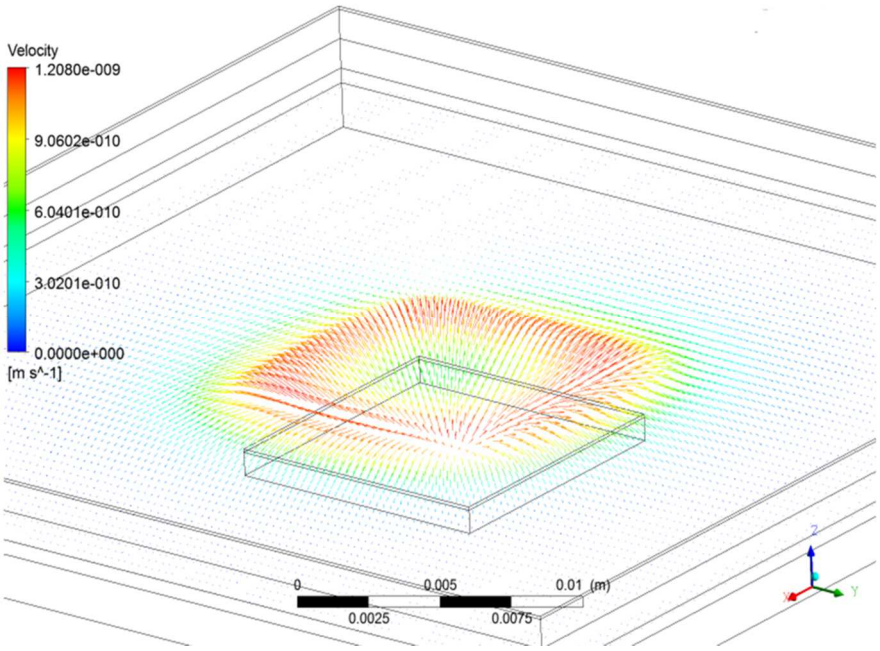

Figure 4-9: Velocity Profile of the Fluid inside the Wick

4.3 Effect of Heat Density and Chip Orientation on the Vapor Chamber Performance

In this section, emphasis is on the effect of heat density and chip orientation on the performance of the vapor chamber. The goal is to find out how significant the configuration of the heat sources and heat distribution among them can affect the vapor chamber performance and junction temperature.

Two different cases are considered in which the total 100 W/cm^2 heat flux is distributed among the three chips. The heat fluxes are 25, 25 and 50W/cm^2 for the first case and 33, 33, 34W/cm^2 for the second case. To investigate the effect of chip orientation, 11 different configurations are considered for each case. Temperature profiles of different configurations for case one and two are shown in figure 4-10 and 4-11 respectively.

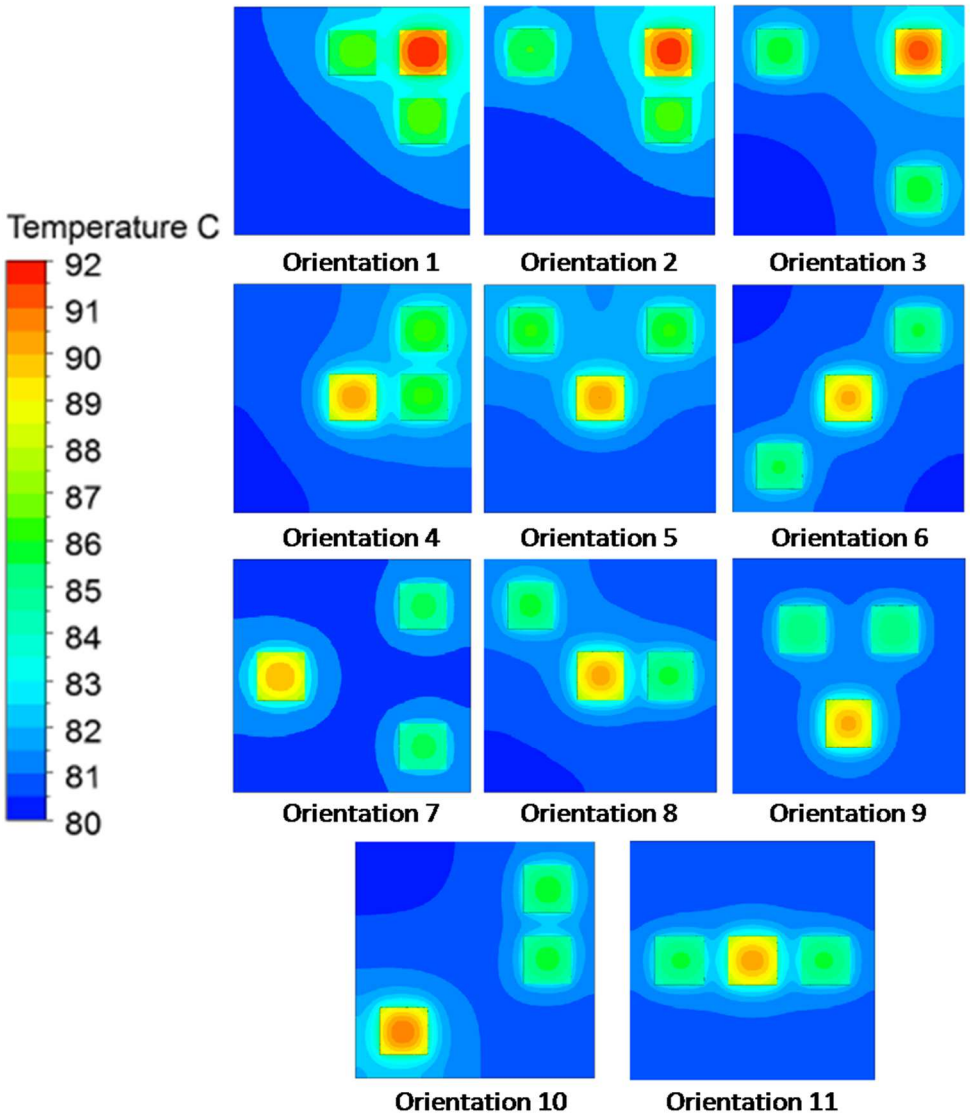

Figure 4-10: Temperature Distribution for Different Chip Orientations (Case 1)

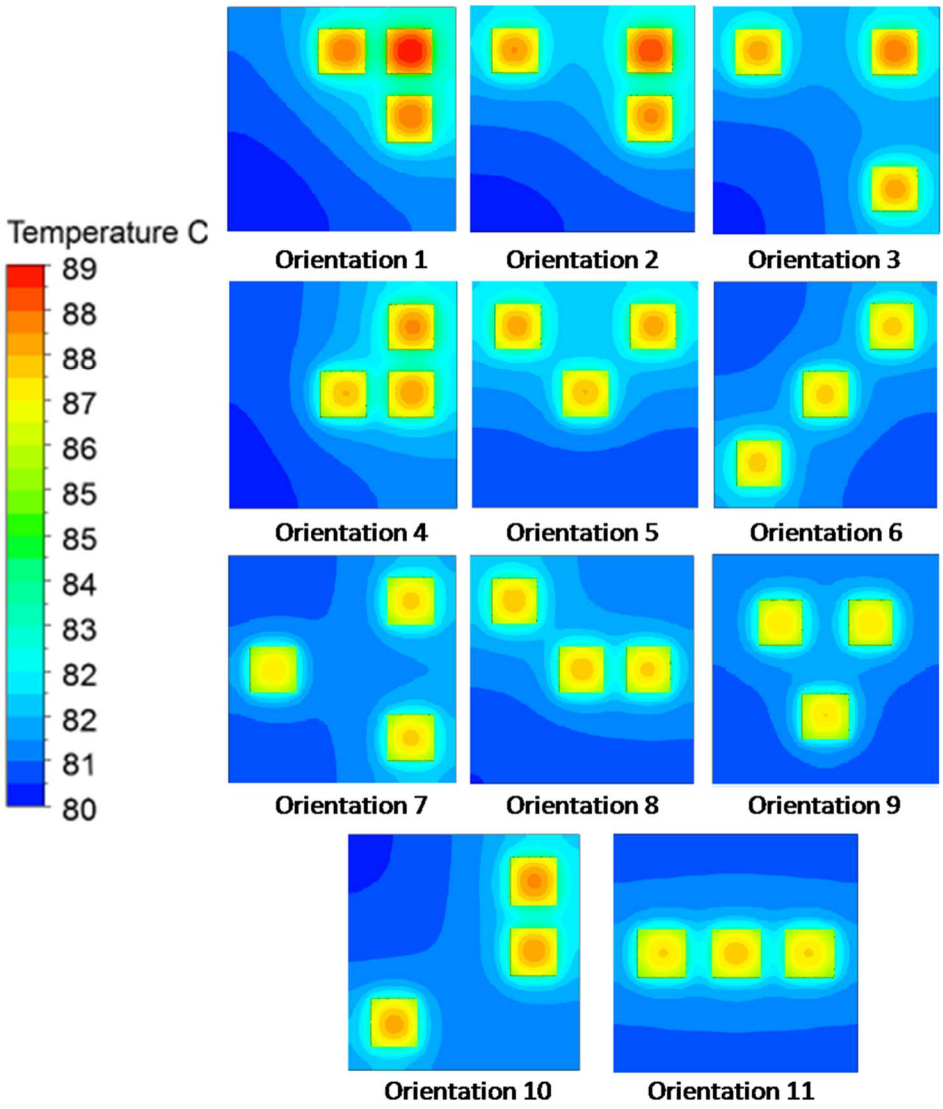

Figure 4-11: Temperature Distribution for Different Chip Orientations (Case 2)

Table 4-1 shows the maximum temperature for all cases. Results show that the maximum temperature is much lower when the total heat flux is distributed almost equally between the chips than the case in which one of the chips accepts half of the total heat flux. It is also seen that the chips experience higher temperature when they are close to

each other at the edges such as orientation 1. One of the desirable configurations is orientation 7 in which the chips are set far from each other and close to edges. Orientation 9 is another desirable setup. In this orientation, the chips are close to each other at the center. These results show that for the same vapor chamber, by choosing the right orientation and heat distribution the maximum temperature can be reduced from 92˚C (worst case) to 86˚C (best case). Therefore, the heat density on the chips and their orientation play an important role in the performance of the vapor chamber and should be considered in designing microelectronic devices.

Table 4-2: Maximum Temperature for Different Orientation and Heat Flux Distribution

Orientation	Temperature ˚C	
	Case 1 (25,25,50 W/cm^2)	Case 2 (33,33,34 W/cm^2)
1	92.3	87.6
2	92.1	87.2
3	91.7	86.1
4	89.5	86.9
5	89.6	86.7
6	89.2	86.4
7	89.2	86.3
8	89.4	86.5
9	89.2	86.2
10	90.6	86.9
11	90.5	86.4

4.4 Transient Analysis

In this section, transient thermal performance of the vapor chamber will be investigated. The initial temperature for the entire vapor chamber is considered to be equal to the ambient temperature which is 35˚C. The velocity of the fluid inside the wick structure is assumed to be zero at t=0s. By doing so, a transient thermal simulation model is developed. Figure 4-12 shows temperature distribution for six different time steps for the single heat source scenario.

The plots are captured at 0, 6, 12, 18, 24, 30 and 36s respectively. As it is seen from the figures, the vapor chamber temperature is uniform and equal to 35˚C at t=0s and starts increasing when the heat is applied to the chip. In the first 6 seconds, the maximum temperature which is the chip temperature increases rapidly and reaches to 78˚C. The chip temperature at t=12s is 89˚C and eventually, the junction temperature reaches to 100˚C around t=36s and the steady state mode starts there.

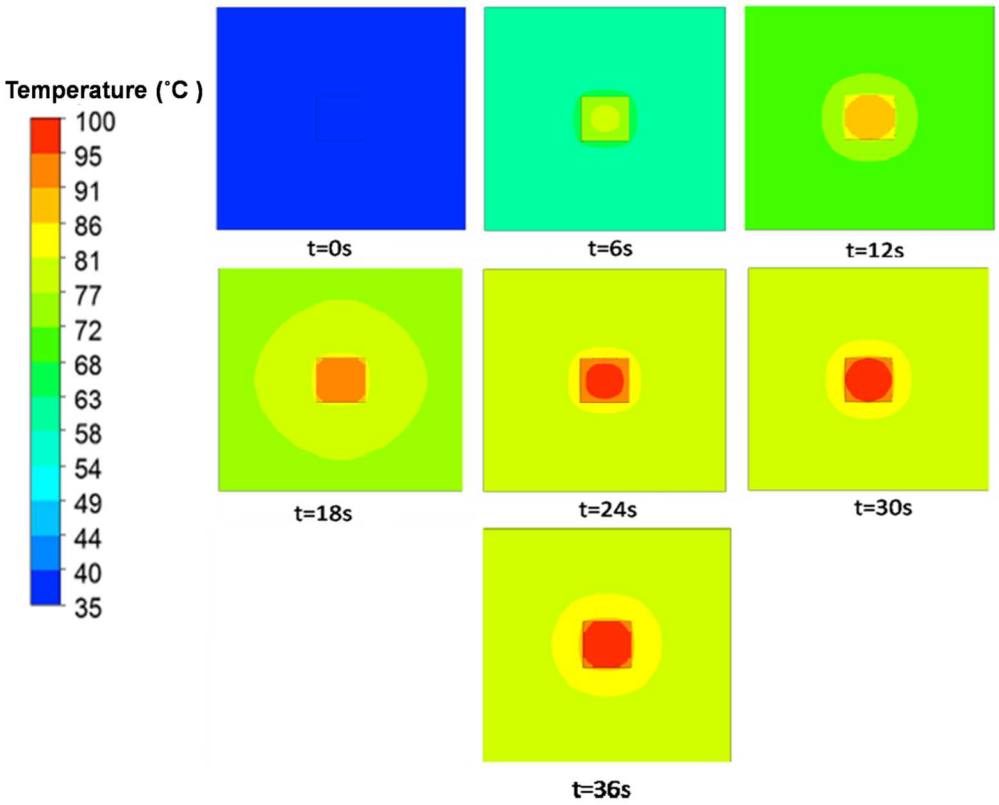

Figure 4-12: Temperature Distribution at Different Time Steps (Single Chip Scenario)

Same procedure is used for a vapor chamber cooling multiple low power heat sources and the results are shown in figure 4-13.

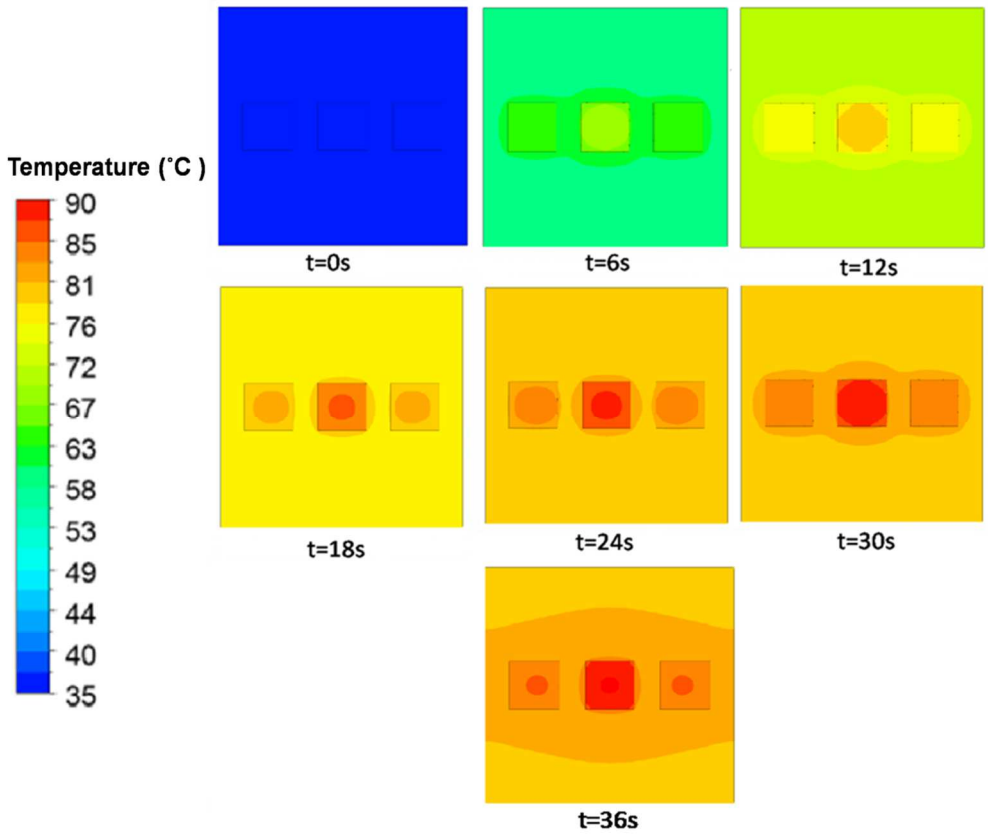

Figure 4-13: Temperature Distribution at Different Time Steps (Multiple Chip Scenario)

A transient comparison of the maximum junction temperature between single and multiple chips scenarios is shown in figure 4-14. The plot shows the temperature of the center of the chip during 60 seconds. It can be seen that the chip temperature increases with almost same rate for both cases and the steady state zone starts from around t=36s.

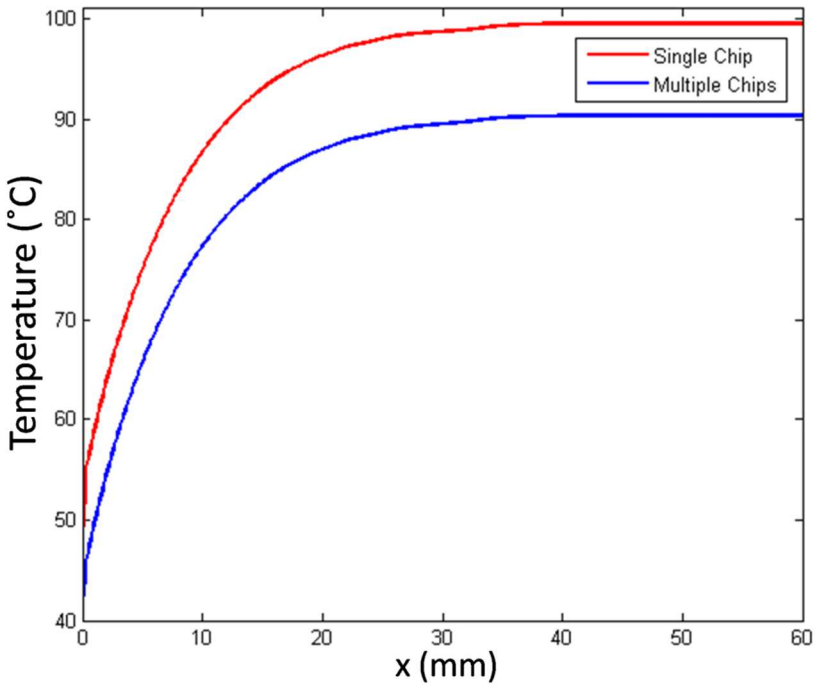

Figure 4-14: Variation of Maximum Temperature with Respect to Time for Single and Multiple Chips

4.4.1 Vapor Chamber vs. Copper and Aluminum Heat Spreaders

In this section, thermal performance of the vapor chamber will be compared with traditional copper and aluminum heat spreaders. In order to do the comparison, copper and aluminum blocks of the same size of the vapor chamber is considered. All boundary conditions are the same as the previous simulation. By doing so, a transient comparison between the thermal performances of vapor chamber, copper block and aluminum block is shown in figure 4-15.

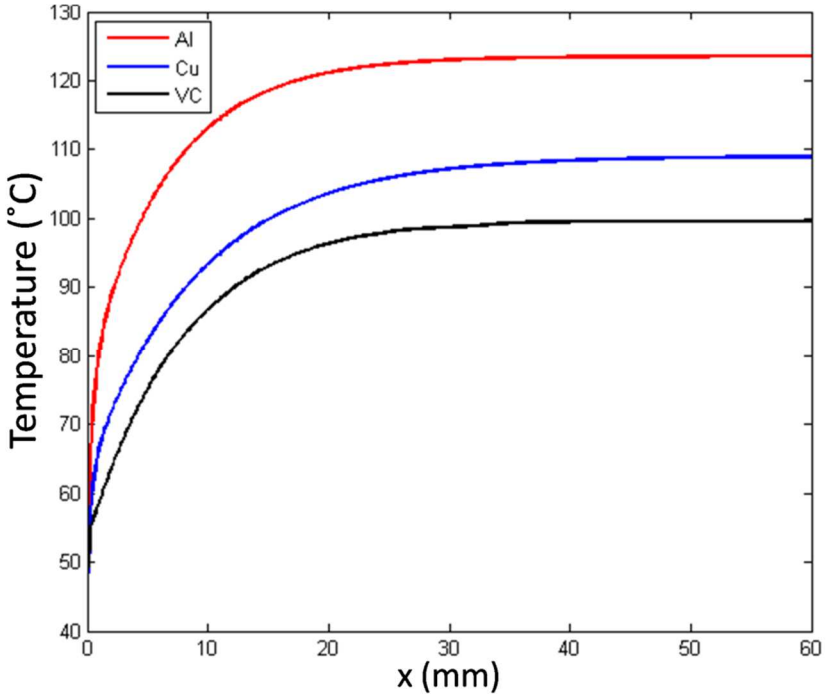

Figure 4-15: Transient Performance of Vapor chamber, Copper and Aluminum Heat Spreaders

It is seen that the maximum temperature for vapor chamber, copper and aluminum are 100, 109 and 124 ˚C, respectively. Therefore, vapor chamber out-performs the copper and aluminum heat spreaders.

Chapter 5

Conclusions and Future Work

5.1 Conclusions

In this thesis, steady state and transient thermal performance of a vapor chamber was investigated. Pure conduction and multi-physics vapor chamber models were developed and compared with each other. Vapor chamber performance for the increasingly common scenario of multiple chips was evaluated. Results indicate that, using a system of low power chips instead of a single high power chip will reduce the junction temperature and increase the performance of the vapor chamber. Effects of heat density and chip orientation on the vapor chamber performance were studied. This data point is important, confirming the correctness and accuracy of the developed models. Moreover, by placing the chips close to each other at the center or far from each other at the edges and equally distributing the total heat flux among them, the junction temperature can be reduced considerably. This conclusion can be used as a guideline for chip designers and/or motherboard designers towards optimizing placement of the chips so that they can be effectively cooled via a vapor chamber.

5.2 Future Work

5.2.1 Addressing the Present Model Limitations

The multi-physics model presented in this study still has some limitations. It is not able to capture the phase change phenomena and the vapor flow inside the vapor space. Therefore, future study is needed to develop a model which is able to account for the entire working fluid motion inside the vapor chamber. However, it is necessary to keep the model simple so it can be used easily for day to day engineering purposes.

5.2.2 Investigating of Mechanical and Electrical Performances

Thermal design is one of the several considerations needed for effective design of microelectronic devices and packaged systems. Future work is needed to investigate other factors that influence the performance of vapor chamber such as mechanical stresses and electrical performance. An optimal design of a complete electronic package embedded with vapor chamber needs to consider the various trade-offs between these aspects of performance.

5.2.3 Using Nanofluids as the Working Fluid

As it mentioned before, depends on the application and required maximum temperature, different types of working fluids may be used. Previous studies focused on using regular fluids such as water, methanol, acetone, lithium, etc. It would be interesting to investigate the effect of using nanofluids as the working fluid inside the wick structure.

5.2.4 Providing a General Design Guideline

Investigation of the thermal performance of a vapor chamber integrating with n number of dies with different sizes, heat densities and orientations can provide a general design guideline for thermal architects.

References

1. Bar-Cohen, A., Kraus, A. D., & Davidson, S. F. (1983). Thermal frontiers in the design and packaging of microelectronic equipment. *MechEng*, *105*(6), 53-59.

2. Dunn, P. D., &Reay, D. (2012). *Heat pipes*. Elsevier.

3. Thomson, M., Ruel, C., &Donato, M. (1989). Characterization of a flat plate heat pipe for electronic cooling in a space environment. In *Proceedings of the 1989 National Heat Transfer Conference, Heat Transfer in Electronics HTD*(Vol. 111, pp. 59-65).

4. Chaudhry, H. N., Hughes, B. R., &Ghani, S. A. (2012). A review of heat pipe systems for heat recovery and renewable energy applications. *Renewable and Sustainable Energy Reviews*, *16*(4), 2249-2259.

5. Yau, Y. H., &Ahmadzadehtalatapeh, M. (2010). A review on the application of horizontal heat pipe heat exchangers in air conditioning systems in the tropics.*Applied Thermal Engineering*, *30*(2), 77-84.

6. Garimella, S. V., &Sobhan, C. B. (2001). Recent advances in the modeling and applications of nonconventional heat pipes. *Advances in Heat Transfer*, *35*, 249-308.

7. A. Faghri, Review and advances in heat pipe science and technology, Journal of Heat Transfer 134 (2012) 123001

8. http://www.coolermaster.com/company/newsDetail-M13032500025534-20121221.html?page=8

9. Faghri, A. (2012). Review and advances in heat pipe science and technology.*Journal of heat transfer*, *134*(12), 123001.

10. Zuo, Z. J., &Faghri, A. (1998). A network thermodynamic analysis of the heat pipe. *International Journal of Heat and Mass Transfer*, *41*(11), 1473-1484.

11. Prasher, R. S. (2003). A simplified conduction based modeling scheme for design sensitivity study of thermal solution utilizing heat pipe and vapor chamber technology. *Journal of Electronic Packaging*, *125*(3), 378-385.

12. Chang, J. Y., Prasher, R. S., Prstic, S., Cheng, P., & Ma, H. B. (2008). Evaporative thermal performance of vapor chambers under nonuniform heating conditions. *Journal of Heat Transfer*, *130*(12), 121501.

13. Take, K., & Webb, R. L. (2001). Thermal performance of integrated plate heat pipe with a heat spreader. *Journal of Electronic Packaging*, *123*(3), 189-195.

14. Vafai, K., & Wang, W. (1992). Analysis of flow and heat transfer characteristics of an asymmetrical flat plate heat pipe. *International journal of heat and mass transfer*, *35*(9), 2087-2099.

15. Zhu, N., &Vafai, K. (1998). Analytical modeling of the startup characteristics of asymmetrical flat-plate and diskshaped heat pipes. *International Journal of Heat and Mass Transfer*, *41*(17), 2619-2637.

16. Wang, Y., &Vafai, K. (2000). Transient characterization of flat plate heat pipes during startup and shutdown operations. *International Journal of Heat and Mass Transfer*, *43*(15), 2641-2655.

17. Lefèvre, F., &Lallemand, M. (2006). Coupled thermal and hydrodynamic models of flat micro heat pipes for the cooling of multiple electronic components. *International Journal of Heat and Mass Transfer*, *49*(7), 1375-1383.

18. Aghvami, M., &Faghri, A. (2011). Analysis of flat heat pipes with various heating and cooling configurations. *Applied Thermal Engineering*, *31*(14), 2645-2655.

19. Wei, X., &Sikka, K. (2006, May). Modeling of vapor chamber as heat spreading devices. In *Thermal and Thermomechanical Phenomena in Electronics Systems, 2006. ITHERM'06. The Tenth Intersociety Conference on*(pp. 578-585). IEEE.

20. Zhu, N., &Vafai, K. (1998). Vapor and liquid flow in an asymmetrical flat plate heat pipe: a three-dimensional analytical and numerical investigation.*International Journal of Heat and Mass Transfer*, *41*(1), 159-174.

21. Vadakkan, U., Chrysler, G. M., & Sane, S. (2005, March). Silicon/water vapor chamber as heat spreaders for microelectronic packages. In *Semiconductor Thermal Measurement and Management Symposium, 2005 IEEE Twenty First Annual IEEE* (pp. 182-186). IEEE.

22. Tien, C. L., &Rohani, A. R. (1974). Analysis of the effects of vapor pressure drop on heat pipe performance. *International Journal of Heat and Mass Transfer*, *17*(1), 61-67.

23. Issacci, F., Catton, I., Heiss, A., &Ghoniem, N. M. (1989). Analysis of heat pipe vapor dynamics. *Chemical Engineering Communications*, *85*(1), 85-94.

24. Vadakkan, U., Murthy, J. Y., &Garimella, S. V. (2003, January). Transient analysis of flat heat pipes. In *ASME 2003 Heat Transfer Summer Conference*(pp. 507-517). American Society of Mechanical Engineers.

25. Carbajal, G., Sobhan, C. B., Peterson, G. P., Queheillalt, D. T., & Wadley, H. N. G. (2006). Thermal response of a flat heat pipe sandwich structure to a localized heat flux. *International Journal of Heat and Mass Transfer*, *49*(21), 4070-4081.

26. Chen, Y. S., Chien, K. H., Wang, C. C., Hung, T. C., & Pei, B. S. (2006). A simplified transient three-dimensional model for estimating the thermal performance of the vapor chambers. *Applied thermal engineering*, *26*(17), 2087-2094.

27. Chen, Y. S., Chien, K. H., Hung, T. C., Wang, C. C., Ferng, Y. M., & Pei, B. S. (2009). Numerical simulation of a heat sink embedded with a vapor chamber and

calculation of effective thermal conductivity of a vapor chamber. *Applied Thermal Engineering*, *29*(13), 2655-2664.

28. Wei, J., Chan, A., & Copeland, D. (2003, March). Measurement of vapor chamber performance [heatsink applications]. In *Semiconductor Thermal Measurement and Management Symposium, 2003. Ninteenth Annual IEEE* (pp. 191-194). IEEE.

29. Wong, S. C., Huang, S. F., & Hsieh, K. C. (2011). Performance tests on a novel vapor chamber. *Applied Thermal Engineering*, *31*(10), 1757-1762.

30. Koito, Y., Motomatsu, K., Imura, H., Mochizuki, M., & Saito, Y. (2003, November). Fundamental investigations on heat transfer characteristics of heat sinks with a vapor chamber. In *Proceedings of the 7th international heat pipe symposium* (pp. 247-251).

31. Koito, Y., Imura, H., Mochizuki, M., Saito, Y., & Torii, S. (2006). Fundamental Experiments and Numerical Analyses on Heat Transfer Characteristics of a Vapor Chamber: Effect of Heat Source Size.

32. Wang, Y., &Vafai, K. (2000). An experimental investigation of the thermal performance of an asymmetrical flat plate heat pipe. *International Journal of Heat and Mass Transfer*, *43*(15), 2657-2668.

33. Wang, Y., &Vafai, K. (2000). An experimental investigation of the transient characteristics on a flat-plate heat pipe during startup and shutdownoperations.*Journal of heat transfer*, *122*(3), 525-535.

34. Maxwell, J. C. (1881). *A treatise on electricity and magnetism* (Vol. 1). Clarendon press.

35. Chi, S. W. (1976). Heat pipe theory and practice: a sourcebook.

36. Grubb, K. (1999, May). CFD Modeling of a Therma-Base (TM) Heat Sink. In *8th International FLOTHERM User Conference* (pp. 13-14).

Biographical Information

Mohammad Parhizi completed his master's degree in Mechanical Engineering at the University of Texas at Arlington. His focus area is in thermal management of microelectronics. He received his bachelor's degree in Mechanical Engineering department at Guilan University in 2012, Rasht, Iran.